JOURNAL OF GEOPHYSICAL RESEARCH, VOL. 103, NO. D24, PAGES 31,783–31,808, DECEMBER 27, 1998

Smoke, Clouds, and Radiation–Brazil (SCAR-B) experiment

Y. J. Kaufman,[1] P. V. Hobbs,[2] V. W. J. H. Kirchhoff,[3] P. Artaxo,[4] L. A. Remer,[1,5]
B. N. Holben,[6] M. D. King,[7] D. E. Ward,[8] E. M. Prins,[9] K. M. Longo,[4]
L. F. Mattos,[3] C. A. Nobre,[3] J. D. Spinhirne,[1] Q. Ji,[5] A. M. Thompson,[1]
J. F. Gleason,[1] S. A. Christopher,[10] and S.-C. Tsay[1]

Abstract. The Smoke, Clouds, and Radiation–Brazil (SCAR-B) field project took place in the Brazilian Amazon and cerrado regions in August–September 1995 as a collaboration between Brazilian and American scientists. SCAR-B, a comprehensive experiment to study biomass burning, emphasized measurements of surface biomass, fires, smoke aerosol and trace gases, clouds, and radiation, their climatic effects, and remote sensing from aircraft and satellites. It included aircraft and ground-based in situ measurements of smoke emission factors and the compositions, sizes, and optical properties of the smoke particles; studies of the formation of ozone; the transport and evolution of smoke; and smoke interactions with water vapor and clouds. This overview paper introduces SCAR-B and summarizes some of the main results obtained so far. (1) Fires: measurements of the size distribution of fires, using the 50 m resolution MODIS Airborne Simulator, show that most of the fires are small (e.g., 0.005 km^2), but the satellite sensors (e.g., AVHRR and MODIS with 1 km resolution) can detect fires in Brazil which are responsible for 60–85% of the burned biomass; (2) Aerosol: smoke particles emitted from fires increase their radius by as much as 60% during their first three days in the atmosphere due to condensation and coagulation, reaching a mass median radius of 0.13–0.17 μm; (3) Radiative forcing: estimates of the globally averaged direct radiative forcing due to smoke worldwide, based on the properties of smoke measured in SCAR-B (-0.1 to -0.3 W m^{-2}), are smaller than previously modeled due to a lower single-scattering albedo (0.8 to 0.9), smaller scattering efficiency (3 m^2 g^{-1} at 550 nm), and low humidification factor; and (4) Effect on clouds: a good relationship was found between cloud condensation nuclei and smoke volume concentrations, thus an increase in the smoke emission is expected to affect cloud properties. In SCAR-B, new techniques were developed for deriving the absorption and refractive index of smoke from ground-based remote sensing. Future spaceborne radiometers (e.g., MODIS on the Earth Observing System), simulated on aircraft, proved to be very useful for monitoring smoke properties, surface properties, and the impacts of smoke on radiation and climate.

1. Introduction

Biomass burning in the tropics is one of the most important, although poorly quantified, human impacts on the environment. Tropical biomass burning now comprises about 80% of the biomass that is burned globally [*Hao and Liu*, 1994]. This is much higher than a century or two ago, due to increases in population in the tropical regions, steady encroachment on forested areas, and the use of controlled burning as a land management tool. Nevertheless, human impacts on the environment through fire are not new. Measurements of charcoal and pollen sediments show a clear correlation between rate of burning, human settlements, and a shift in the natural vegetation from pyrophobic to pyrotolerant and pyrophilic species [*Crutzen and Andreae*, 1990, hereinafter referred to as CA90].

Scientific interest in tropical biomass burning was heightened some two decades ago with the suggestion by *Crutzen et al.* [1979, 1985] that it is an important source of some key trace gases in the atmosphere. It is now known that biomass burning is responsible for 10–30% of the global CO budget, which is of particular importance since the emissions are in the tropics, a region of strong solar radiation, including UV, and therefore of major importance for tropospheric chemical processes [CA90]. CO, through interactions with the OH radical, can substantially reduce the oxidative (or cleansing) efficiency of the atmosphere; biomass burning may therefore increase the lifetime and concentrations of many trace gases [CA90]. In

[1]Laboratory for Atmospheres, NASA Goddard Space Flight Center, Greenbelt, Maryland.
[2]Department of Atmospheric Sciences, University of Washington, Seattle.
[3]Instituto de Pesquisas Espaciais (INPE), São José dos Campos, São Paulo, Brazil.
[4]Instituto de Fisica, Universidade de São Paulo, São Paulo, Brazil.
[5]Science Systems and Applications Inc., Lanham, Maryland.
[6]Laboratory for Terrestrial Physics, NASA Goddard Space Flight Center, Greenbelt, Maryland.
[7]Earth Sciences Directorate, NASA Goddard Space Flight Center, Greenbelt, Maryland.
[8]Intermountain Research Station, Forest Service, USDA, Missoula, Montana.
[9]National Oceanic and Atmospheric Administration/NESDIS/ORA, Madison, Wisconsin.
[10]Department of Atmospheric Sciences, University of Alabama in Huntsville, Huntsville.

Paper number 98JD02281.
0148-0227/98/98JD-02281$09.00

regions of biomass burning, oxidation of CO and hydrocarbons in the presence of elevated concentrations of NO_x causes formation of ozone in concentrations as high as in strongly polluted urban smogs [*Kirchhoff*, 1984; *Logan and Kirchhoff*, 1986; CA90]. Since NO_x has a lifetime of only a few days (similar to the lifetime of smoke aerosol), and CO of 10 to 100 days, the high NO_x concentration from biomass burning is mainly in smoke regions. Biomass burning is also a source of CH_4 [CA90].

Biomass burning is also a major source of atmospheric aerosol. It emits submicron particles composed mainly of partially oxidized organic materials. These particles are both efficient scatterers and absorbers of sunlight. They are also efficient cloud condensation nuclei (CCN) and therefore interact with clouds [*Warner and Twomey*, 1967; *Hobbs and Radke*, 1969; *Holben et al.*, 1991; *Kaufman et al.*, 1992]. The global rate of production of biomass burning aerosol is not much smaller than the global rate of production of sulfate aerosol [*Radke*, 1989]. The possible climatic effects of smoke particles was pointed out by *Crutzen et al.* [1985] and provided the basis for the "nuclear winter" hypothesis [*Crutzen and Birks*, 1982], in which smoke from fires caused by a nuclear attacker was hypothesized to diminish sunlight and agricultural productivity over the entire hemisphere. Heavy smoke in northern latitudes is known to reduce daytime ground temperature by several degrees [*Robock*, 1988]. Emission of smoke particles is estimated to have a similar direct effect (through interaction with solar radiation) and indirect effect (through interacting with clouds that reflect sunlight) on the Earth's radiation balance to that of sulfates [*Penner et al.*, 1992]. However, recent revised estimates of the radiative forcing of smoke worldwide, based on measurements from SCAR-B, are significantly lower both for the direct [*Hobbs et al.*, 1997] and the indirect [*Kaufman and Fraser*, 1997] effects. Nevertheless, the effect of smoke on radiation, cloud microstructure, and air pollution are of major importance on local and regional scales. The effects of smoke on atmospheric temperature profiles and cloud microstructures may disturb the hydrological cycle in the tropics, with potential effects on regional and global climate. Long-range transport fueled by convective injection into higher altitudes has been documented [*Pickering et al.*, 1996; *Fishman et al.*, 1996], but the effects on global climate and atmospheric chemistry are not well established. Other important impacts of biomass burning on regional environments were reviewed by CA90. They include acid deposition, effects on soil degradation and nutrient cycle, deforestation, and effects on local biota, animals, and people.

Early field studies of biomass burning in the tropics emphasized measurements of the emission of trace gases and their evolution in the atmosphere, particularly the formation of tropospheric ozone. These included measurements in Brazil by *Crutzen et al.* [1985], *Andreae et al.* [1988], and *Fishman et al.* [1996], and in Africa by *Lindesay et al.* [1996] and *Lacaux et al.* [1995]. Studies of biomass burning that have placed more emphasis on the properties of the smoke aerosol in North America include those of *Radke et al.* [1991], *Ward and Hardy* [1991], and *Hobbs et al.* [1996]; in Brazil by *Holben et al.* [1991], *Kaufman et al.* [1992], *Ward et al.* [1992], *Artaxo et al.* [1996], *Pereira et al.* [1996], *Browell et al.* [1996]; and in Africa by *Andreae et al.* [1994], *Anderson et al.* [1996], *Le Canut et al.* [1996], *Maenhaut et al.* [1996], *Kuhlbusch et al.* [1996], *Ward et al.* [1996], and *Swap et al.* [1996]. A network of Sun/sky radiometers has operated in Brazil since 1993 [*Holben et al.*, 1996; *Kaufman and Holben*, 1996; *Remer et al.*, 1996, this issue] in an effort to characterize the aerosol properties and to develop methods for remote sensing from space of fires, smoke aerosol, and their impact on clouds [*Kaufman et al.*, 1990, 1994, 1998; *Kaufman and Fraser*, 1997].

There are many uncertainties in the rates of biomass burning, its spatial and temporal distributions, the emission of particles and trace gases, and the atmospheric and radiative processes and effects associated with smoke. The horizontal and vertical heterogeneities in the distribution of smoke, its variability with time, and the presence of many small sources (see Plates 1 and 2) increase the difficulty in estimating the rate of biomass burning and its effects on climate. Recent interest in the climatic effects of smoke [CA90; *Penner et al.*, 1992; *IPCC*, 1995; *Seinfeld et al.*, 1996] and the new capability of satellite instrumentation to measure aerosols and their interactions with water vapor, clouds, and radiation (POLDER on ADEOS [*Herman et al.*, 1997a], MODIS on EOS [*Kaufman et al.*, 1997; *Tanré et al.*, 1997], and MISR on EOS [*Martonchik and Diner*, 1992; *Kahn et al.*, 1997]) have generated a need for a biomass burning experiment with emphasis on the physical properties and processes associated with smoke emissions and their remote sensing. The SCAR-B experiment in Brazil, which was conceived by American and Brazilian scientists, was designed to meet this need.

In the remainder of this paper, we first describe the goals of SCAR-B. We then review previous studies of biomass burning in Brazil. This is followed by an overview of the SCAR-B measurement program and some of the main results from SCAR-B. Comprehensive accounts of specific aspects and findings of SCAR-B may be found in the papers in this special issue.

2. Goals of SCAR-B

SCAR-B was a comprehensive experiment to measure the emissions of trace gases and aerosol particles from biomass fires in Brazil and their evolution and interactions in the atmosphere. Three main goals guided SCAR-B: (1) characterization of the effects of emissions from biomass burning on direct and indirect forcing of solar radiation; (2) evaluation of the effects of biomass burning on atmospheric chemistry and radiation; and (3) evaluation of remote sensing techniques against in situ measurements, in preparation for the launch of the NASA moderate resolution imaging spectroradiometer (MODIS) on an Earth Observing System AM-1 satellite in 1999.

Some of the more specific objectives of SCAR-B were (1) to establish the thermal properties of fires, their remote sensing from space, and the relationship among fire thermal properties, the emission rates of smoke, and the rate of biomass consumption; (2) to establish the rates of emissions of trace gases and particles (including the effective concentration of black carbon) from biomass burning; (3) to measure the distribution and evolution of trace gases in the atmosphere; (4) to measure the optical/radiative properties of smoke, including scattering and absorption efficiencies, spectral extinction, scattering phase function and single-scattering albedo, the effects of humidity on smoke aerosol size, and the evolution of these properties with smoke age; (5) to develop a physical and radiative model of smoke that can be used for remote sensing of smoke aerosol and for estimating its direct radiative forcing; (6) to understand the interactions of smoke particles with water vapor and clouds; their CCN nucleating efficiency; their

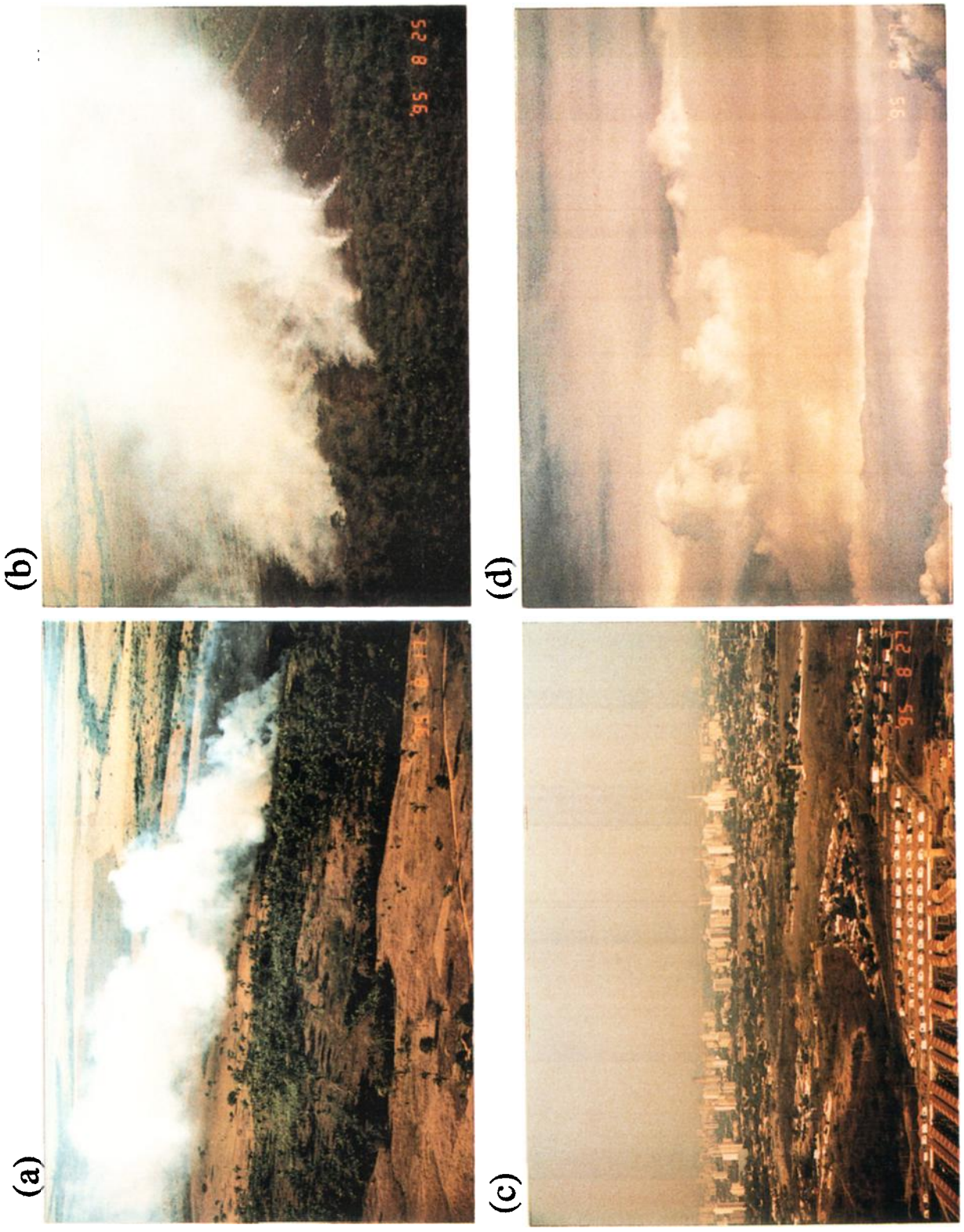

Plate 1. Examples of smoke from biomass burning in Brazil during SCAR-B. (a) A small cerrado fire north of Brasilia. (b) Lines of fire in cerrado northwest of Cuiabá. (c) Regional haze dominated by smoke over Cuiabá. (d) Cumulus clouds produced by fires near Marabá. Note the banded smoke layers. Photos by Peter V. Hobbs.

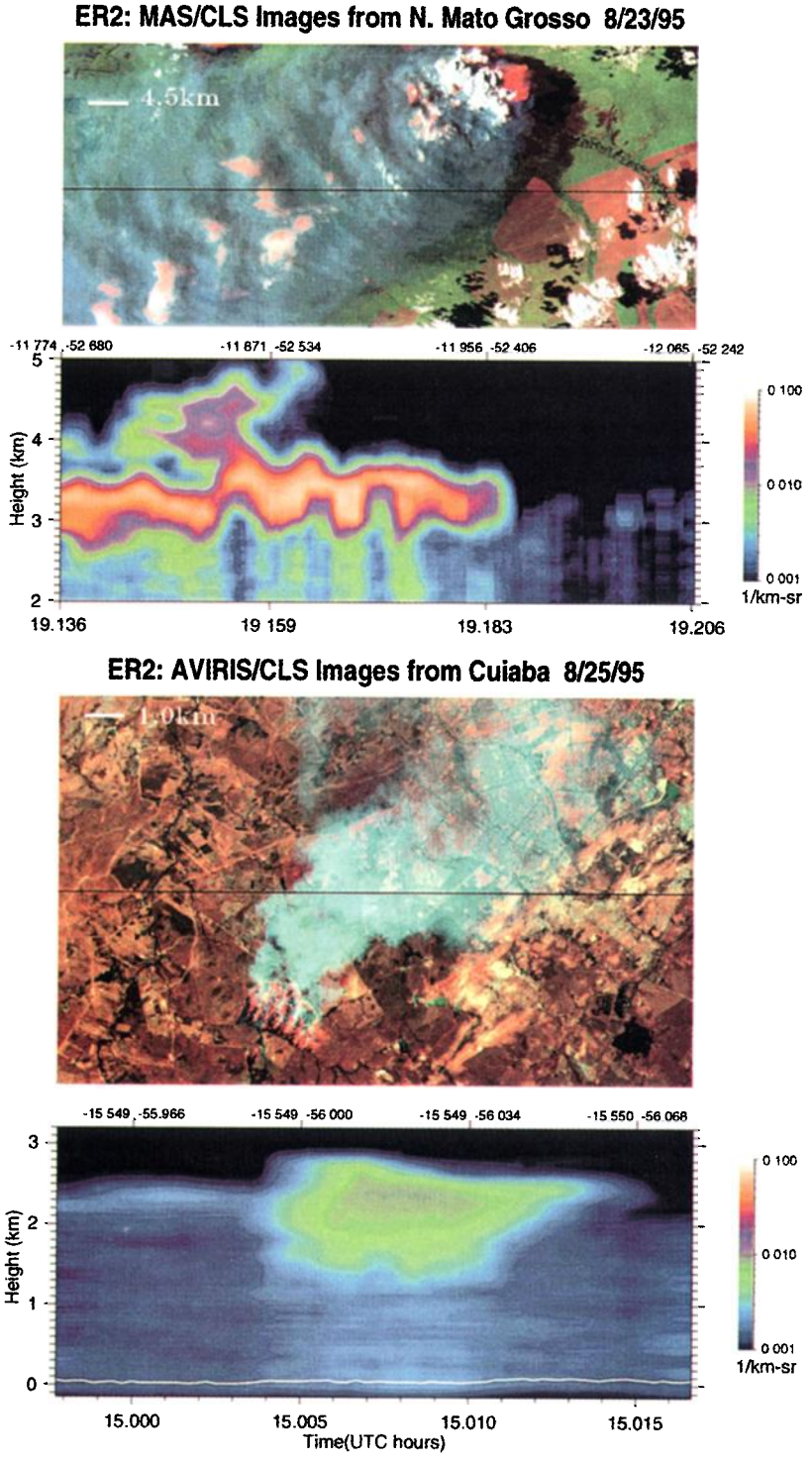

Plate 2. Examples of fires, burn scars, smoke, and clouds observed from the NASA ER-2 aircraft. (Top panels) MAS and lidar images of the landscape in Northern Matto Grosso, Brazil (11.9°S, 52.5°W), showing a large fire of dense biomass emitting smoke into a humid atmosphere at 3–4 km with evident cloud formation (August 23, 1995, at 1910 GMT). The MAS image is composed of the 660 nm channel (blue), the 860 nm channel (green), and the 1650 nm channel (red). The fire is the red spot in the top right part of the image. The orange clouds are darker in the 660 and 860 nm channels due to absorption of smoke above them. The lidar image is the backscattering coefficient measured from the lidar. (Bottom panels) AVIRIS and lidar images of the landscape in Cuiabá, Brazil (9.9°S, 56.1°W) with a large fire of lower-density biomass emitting smoke into a drier atmosphere at 2 km (August 25, 1995 at 1500 GMT); no cloud activity is evident. The AVIRIS image is composed of the 460 nm channel (blue), the 550 nm channel (green), and the 1650 nm channel (red). The fire is in the bottom left part of the image with red fire strips emitting the smoke and black burn scars formed between them.

Table 1. Summary of Field Experiments to Study Smoke From Biomass Burning in Brazil

Experiment	Period	Main Focus	Reference
Brushfire-80	1980	analysis of trace gas and aerosol emissions from biomass burning in Manaus and Rondonia	*Crutzen et al.* [1985]
CAMREX (Carbon in the Amazon River Experiment)	1982–1996	study the carbon and hydrologic cycles	*Richey et al.* [1990]
ARME (Amazon Region Micrometeorological Experiment)	1983–1985	Forest-atmosphere micrometeorological interactions	
ABLE-2A and -2B (Amazon Boundary Layer Experiment)	1985 and 1987	large-scale aircraft measurements of trace gases and aerosol from biomass burning (ABLE-A), and biogenic emissions (ABLE-B)	*Harriss et al.* [1988, 1990]
FLUAMAZ (Atmospheric Fluxes in Amazonia)		water and energy balances for western Amazonia	
BASE-A and -B (Biomass Burning Airborne and Spaceborne Experiment–Amazon and Brazil)	1989 and 1990	emission ratios of trace gases and aerosol particles and their optical properties for calibration of spaceborne estimates of the emissions from biomass burning	*Kaufman et al.* [1992]; *Ward et al.* [1992]
ABRACOS (Anglo-Brazilian Amazonian Climate Observations Study)	1990–1996	CO_2 water, and energy fluxes between the forest and the atmosphere over pasture and primary rain forest	*Gash et al.* [1996]
TRACE-A (Tropical Atmospheric Chemistry Experiment–Atlantic)	1992	atmospheric exchange and formation of ozone from biomass burning emissions in the South Atlantic Ocean	*Fishman et al.* [1996]
FLOR-PAST (Land use Change and Ecosystem Processes in the Brazilian Amazon Basin)	1992–1994	dynamics of the atmospheric boundary layer over deforested areas in Rondonia	
MACOE (Manaus Carbon Observation Experiment)		CO_2 fluxes in a forested area	*Grace et al.* [1995]
SCAR-B (Smoke, Clouds, and Radiation—Brazil)	1995	characterization of fires, emissions of trace gases and aerosol, their evolution, and interactions in the atmosphere with clouds and radiation	this issue
BIONTE (Experiment on Biomass and Nutrients in Terra-Firme Forests in Central Amazonia)	1996	nutrient cycles and biomass in "terra-firme" forests looking at sustainable development strategies	*Mello-Ivo et al.* [1996]

effects on cloud microphysics, cloud reflectance and indirect forcing of climate; and, cloud effects on smoke aerosol size distributions, concentrations, and properties; and (7) to establish the effects of biomass burning on surface reflective properties, albedo, and their remote sensing from space in the presence of smoke.

3. Previous Experiments in Brazil

SCAR-B follows a series of 10 field campaigns on biomass burning and biogenic emissions conducted in Brazil, between 1980 and 1994, and the monitoring of various atmospheric constituents from ground sites. Table 1 summarizes the main objectives of these experiments. The shifting interest from emissions of trace gases and tropospheric chemistry to include the emission of smoke particles and their radiative effects was already reflected in some of the measurements in ABLE-2A [*Andreae et al.*, 1988], it was one of the main objectives of the BASE and TRACE experiments, and it is reflected in the types of measurements obtained in SCAR-B. In the last decade, long-term continuous ground-based measurements have also been conducted in Brazil of aerosol concentration and composition, black carbon concentration, and trace gases and ozone concentrations [*Artaxo et al.*, 1994, this issue; *Kirchhoff*, 1988, 1996]. Continuous monitoring of fires from satellites is also available [*Setzer and Pereira*, 1991].

4. Interannual Variability of Biomass Burning in Brazil

The rate of biomass burning in Brazil, and therefore the amounts of trace gases and aerosols emitted, changes from year to year. Meteorological conditions affect the area of the forests and grass lands that burn each year and the fraction of the biomass consumed in the fire. It is also affected by many social factors. In this section, we discuss various measures of the interannual variability of biomass burning in Brazil and the rates of emissions and formation of pollutants in the atmosphere from this source. This will help put the 1995 SCAR-B

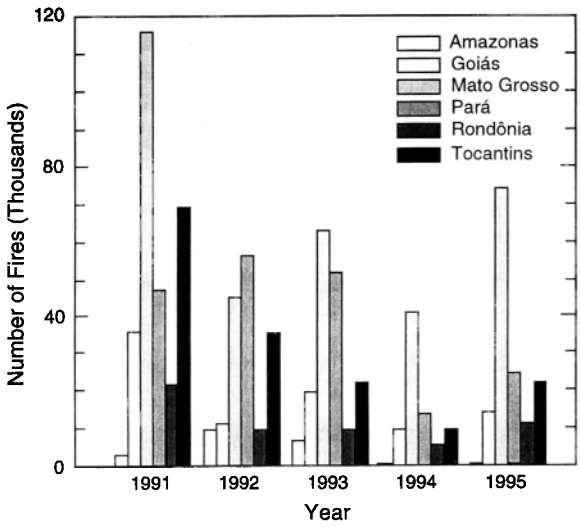

Figure 1. Biomass burning in Brazil from 1991 to 1995 by state (see key) as represented by the AVHRR fire count. The data were collected and processed by INPE. Because of differences in AVHRR instrumentation and observation time in 1994 and 1995 the afternoon and morning satellites were used at the beginning and end of the dry season, respectively. The change in the detection of fire rate between the two orbits was compared in August and corrected (from INPE reports).

measurements into perspective in terms of the longer-term biomass burning record in South America.

4.1. Fires

The advanced very high resolution radiometer (AVHRR) aboard the NOAA satellite can provide daily data on the number of fires in Brazil. The fires are identified in the AVHRR 3750 nm channel [*Setzer and Pereira*, 1991]. The total number of fire pixels for different Brazilian states are summarized in Figure 1. One complication in this multiyear comparison is that different instruments and different satellites have been used. Until August 14, 1995, the afternoon NOAA 14 satellite was used, whereas from August 15 to the end of the burning season in 1995, the morning NOAA 12 satellite was used. A similar procedure was adopted to detect fires in 1994 from two NOAA satellites, but the afternoon NOAA 11 was used first, which was then replaced by the morning NOAA 10. Switching between satellites was dictated by the change in the diurnal passing time of the afternoon satellites, which affected the reflection of sunlight at 3700 nm and the ability to observe the fires. The rate of fire detection from both sensors was compared for the August period and used to recalculate the fire rate. The recalculated fire count is shown in Figure 1. Figure 1 shows that the fire activity in 1995 was in the upper range of fire activity and biomass burning for other years.

4.2. Deforestation

Deforestation accounts for a major part of biomass burning in Brazil [*Skole and Tucker*, 1993]. Figure 2 shows the rate of deforestation in Brazil, based on analysis of Landsat images by the Ministry of Science and Technology, Brazil. For the period 1978–1988 the average estimate of deforestation is plotted. The rate of deforestation in the 1990s is lower than in the 1980s. However, in 1995 the rate of deforestation was double that in previous years and in 1996.

4.3. Emissions of Smoke Particles, Black Carbon and Ozone Formation

During the 1990s, long-term, ground-based monitoring of the emission of trace gases and aerosols from biomass burning was conducted by INPE and the University of São Paulo [*Kirchhoff*, 1988; *Artaxo et al.*, 1988, 1994]. The concentrations of fine and coarse mode particles (under and above 2 μm diameter, respectively) and the equivalent concentrations of black carbon, as derived from absorption measurements, are shown in Figure 3 [*Artaxo et al.*, 1988, 1990, 1994, 1997]. The concentration of smoke particles was high in Alta Floresta in 1995, probably due to enhanced deforestation, but lower in Cuiabá. The black carbon fraction was higher in Cuiabá than in Alta Floresta.

Ozone is a by-product of biomass burning and depends in complex ways on the concentrations of CO, hydrocarbons, NO_x, and the availability of sunlight. Ground-based ozone measurements were made at two sites: Natal, on the eastern corner of northern Brazil, upwind from South American biomass burning, and in air that enters Brazil; and Cuiabá in the center of the cerrado region where smoke concentrations are high due to transport from the north and northeast as well as from local sources [*Kirchhoff*, 1996]. The difference between the diurnal cycle of ground-based ozone at these two sites, shown from 1990 to 1995 in Figure 4, is a clear indication of the effect of biomass burning on daily ozone production. As in the case of the fire count, or the concentration of smoke particles and black carbon in Cuiabá (Figures 1 and 3), the ozone concentrations show that 1995 was in the upper range for biomass burning, similar to 1993 and 1994. In 1992, the year of the TRACE-A experiment, the rainy season arrived earlier. 1992 also had a relatively low fire count (Figure 1) and was a minimal year for smoke and black carbon both in Cuiabá and Alta Floresta. Higher ozone and NO_x concentrations at higher altitudes were detected during the TRACE-A experiment in Natal (not shown) as compared to SCAR-B. These higher concentrations are due to long-range transport from Africa and South America and enhancement by lightning [e.g., *Pick-*

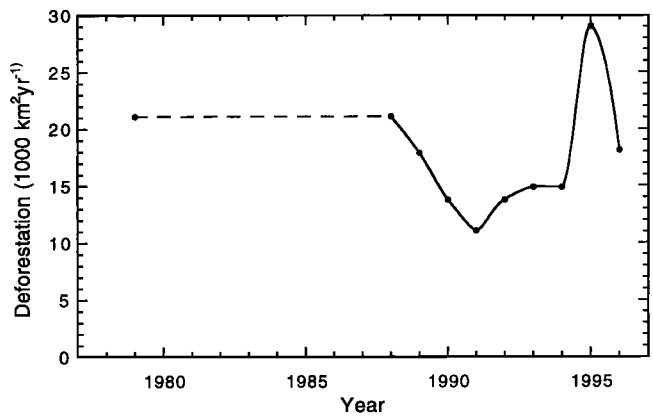

Figure 2. Rate of deforestation in km^2/yr (from INPE/MCT, Ministry of Science and Technology, Brazil). The dashed line between 1979 and 1988 indicates a multiyear average. Note that the reported value for the additional deforestation between two consecutive years (e.g., 1990 and 1991) is plotted for the later year (e.g., 1991). The deforestation during 1995 was significantly larger than during the other years.

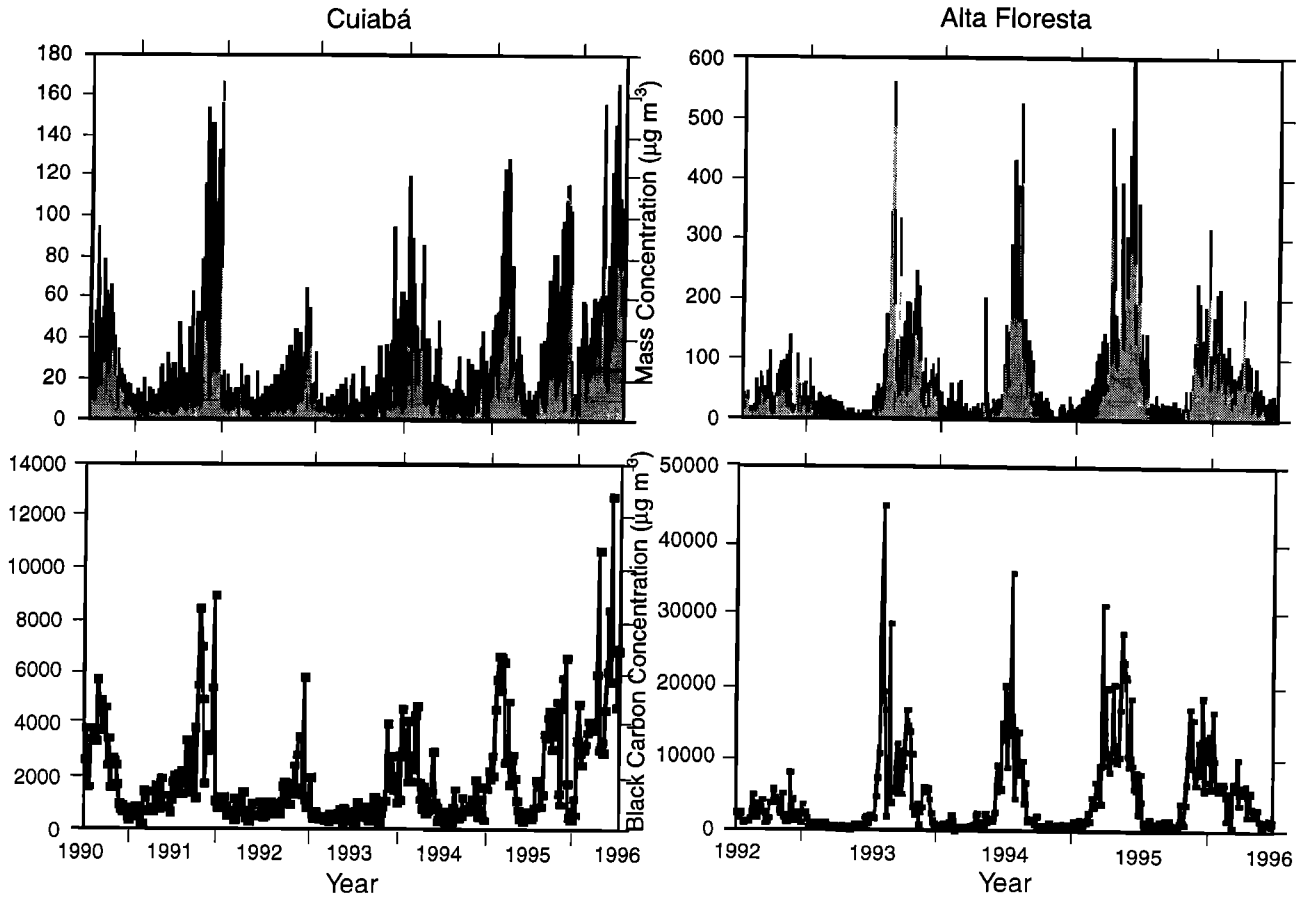

Figure 3. Ground-based measurements of the concentrations of smoke particles (top panels) and equivalent black carbon concentration derived from absorption measurements (bottom panels). The particle concentration ($\mu g\ m^{-3}$) is shown in gray for the fine particle mode (diameter $<2\ \mu m$) and in black for the coarse mode (diameter $>2\ \mu m$). The results for Cuiabá (326 samples), representing cerrado and agricultural fires, collected from 24 July 1990 to 2 September 1996, are shown on the left. The results for Alta Floresta (353 samples), representing deforestation and regrowth fires, are given on the right for the period from August 23, 1992 to October 25, 1996. The concentrations of black carbon were derived from light absorption measurements.

ering et al., 1996; *Thompson et al.*, 1996; *Kirchhoff and Alvalá*, 1996].

4.4. Regional Smoke

Measurements from the Nimbus 7 TOMS instrument can be used to estimate the regional rate of emission of aerosol particles from biomass burning in the Amazon Basin and cerrado. The TOMS instrument measures the effect of aerosol absorption on the scattering of solar ultraviolet radiation from the Earth's atmosphere. Smoke aerosol absorbs ultraviolet radiation, which has a stronger effect on the TOMS 340 nm channel than on the 380 nm channel. This differential absorption is used to derive the aerosol index [*Herman et al.*, 1997b]. The differential absorption and the 380 nm radiance can be used to retrieve the aerosol optical thickness (AOT) at 380 nm, τ_{380} [*Hsu et al.*, 1996; *Torres et al.*, 1998; *Gleason et al.*, this issue]. The AOT retrieval is dependent on aerosol model assumptions and the aerosol scale height. The analysis of the TOMS data is particularly important due to its long-term data record, which was recently integrated and intercalibrated [*Herman et al.*, 1997b]. The area of the Brazilian cerrado and forest covered by smoke is shown in Figure 5 for four thresholds of the smoke optical thickness. Similar smoke aerial coverage data for 1978 through 1995, using multiple satellites, is shown by *Gleason et al.* [this issue]. The integrated smoke loading (given by the product of the smoke area covered by a given smoke optical thickness) is also plotted. The smoke loading varies from year to year by more than 50%. Comparison with the fire count from AVHRR (Figure 1) shows that 1992 had less smoke and fewer fires than 1991. Comparison with the ozone production shown in Figure 4 confirms that 1991 had a stronger biomass burning signal.

4.5. Summary of Interannual Variability

The measures of deforestation, fire frequency, and concentration of emissions, shown in Figures 1–5, provide an overall picture of the interannual variability of biomass burning in Brazil. On the basis of these indicators, it is clear that biomass burning in 1995 was relatively high (see Figures 1, 3, and 4). In particular, the rate of deforestation was large in 1995. An additional common feature shown by these features is the lower rate of biomass burning in 1992.

5. Meteorological Conditions in SCAR-B

A meteorological operations center was set up at the Brazilian office of IBAMA (Instituto Brasileiro do Meio Ambiente

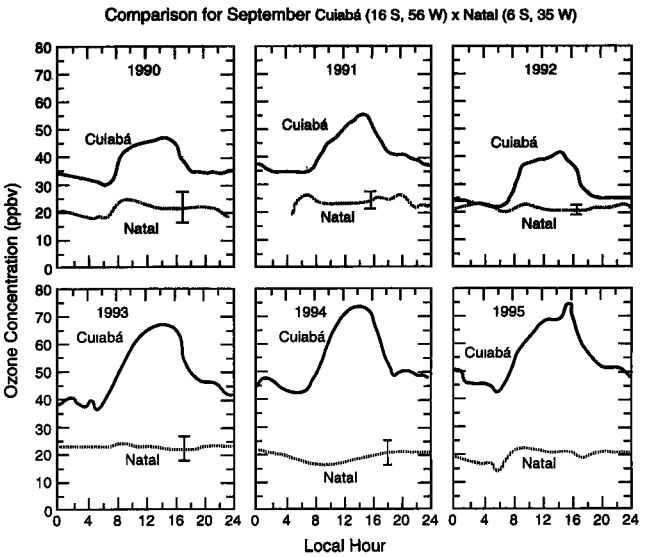

Figure 4. Time evolution of surface ozone concentrations measured at Cuiabá (16°S, 56°W), in the middle of the biomass burning area, and Natal (6°S, 35°W), on the northeastern Atlantic Coast of Brazil. Natal receives air from the east and is therefore not directly affected by smoke from biomass burning. The measurements are for the month of September. A clear tendency for increasing ozone concentration due to biomass burning can be seen (from *Kirchhoff* [1996]).

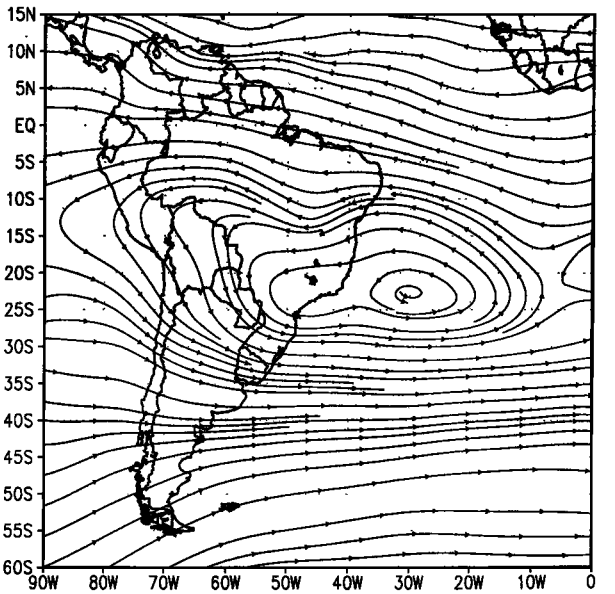

Figure 6. Time-averaged 700 mbar wind field for the SCAR-B period (August 16 to September 10, 1995), derived from four daily (0000, 0600, 1200, and 1800 UTC) National Centers for Environmental Prediction (NCEP) global reanalyses.

e dos Recursos Naturais) to guide the SCAR-B field operations. Data from the INPE meteorological center, Centro de Previsao de Tempo e Estudos Climaticos (CPTEC), and GOES 8 satellite data analyzed for smoke, clouds, and fire

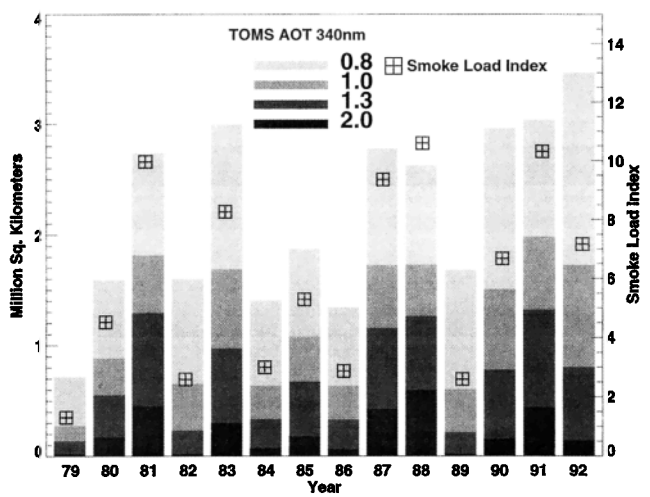

Figure 5. Long-term smoke measurements from TOMS. The gray bars show the area covered by smoke with TOMS-detected aerosol optical thickness (AOT) at a wavelength of 340 nm exceeding a given threshold (shown in the legend). The term "effective" is used for AOT since the measurements depend on assumptions concerning aerosol absorption and vertical profile. The area is used to calculate the total smoke load index (in units of km^2, sum of the products of the effective AOT and the corresponding area covered by it) and is shown by the symbols for each year. The data are detected in an L-shaped box between 40° and 70°W and 2°N and 30°S (see *Gleason et al.* [this issue] for more details).

distribution were obtained electronically and displayed in the SCAR-B operations center in IBAMA. Meteorological forecasts were based on the numerical weather prediction models of CPTEC and the medium-range forecast and aviation models from the U.S. National Center for Environmental Prediction (NCEP). Detailed meteorological information from the INPE meteorological center, CPTEC, and the location and transport of smoke from the GOES satellite images was monitored continuously and used to aid decision making on deployment of the aircraft [*Prins et al.*, this issue; *Nobre et al.*, this issue].

Average streamlines over South America during the August–September 1995 time frame of SCAR-B are shown in Figure 6. The meteorological conditions are described in detail by *Nobre et al.* [this issue] and summarized below. The large-scale systems responsible for the climate in the region covered by SCAR-B are the Intertropical Convergence Zone (ITCZ) in the north, frontal systems (FS) pushing up from the south, and the South Atlantic subtropical high (SASH) off the east coast of Brazil. In the southern hemisphere winter the ITCZ generally migrates northward, reducing large-scale convective rainfall. The FS reach their lowest latitudes in South America during this season; however, they bring cold surges without convective activity. The combination of these two factors creates a typically dry region over most of Brazil during the southern hemisphere winter, called the "dry season."

During the dry season, the SASH drifts back toward the continent from its wet season location in the mid-Atlantic (see Figure 6 for the conditions in the dry season). Together with the presence of the Andes, the SASH generates the air circulation shown in Figure 6. East winds dominate the northern parts of the SCAR-B area. The western part has northern winds with lower speeds, higher temperatures, and lower pressure. The anticyclonic circulation persists throughout the lower troposphere to an altitude of 5 km, causing long periods of little cloudiness. This system was dominant during SCAR-B,

blocking and diverting the FS at lower latitudes toward the ocean. The anticyclonic pattern creates high-level subsidence that decreases humidity and results in stagnant conditions conducive to the formation of hazes in the boundary layer. During August and the first half of September 1995 a strong SASH generated higher temperature and lower humidity than usual, which virtually eliminated convective activity in the central area of the cerrado. The result was a very dry season and high incidences of fires and smoke, as evident in Figures 2 and 4. After the termination of SCAR-B on 15 September the SASH weakened and cloudiness increased.

Trajectory analyses are shown in Plate 3. Forward trajectories (Plate 3a) show mostly stagnant conditions that initially kept the smoke close to the source regions but then eventually transported the smoke from the major biomass burning regions following the anticyclonic flow. Cuiabá, where many of the SCAR-B measurements took place, received smoke from the north and northeast and maritime and urban air from the southeast and southwest (Plate 3b). The origin of the air mass up to 800 mbar over the central cerrado area was predominantly from the east but with occasional bursts from the northern and even southern quadrants [*Freitas et al.*, 1996; *Longo et al.*, 1998]. There is an apparent contradiction between the trajectory analysis, which shows transport over the Atlantic, and the analysis of AVHRR data for aerosol over the ocean, which does not show this transport [*Husar et al.*, 1997]. This is due to the association of the transport of the smoke with heavy clouds. Analysis of GOME data (Plate 3) during the SCAR-B experiment (GOME observes smoke in a similar fashion to TOMS) shows substantial transport of smoke to the Atlantic Ocean. The analysis of the GOME ultraviolet data is less sensitive to the presence of clouds and shows, in this case, 10% of the smoke present over the ocean. Analysis of smoke occurrence in GOES images during the dry season of June to October 1995 [*Prins et al.*, this issue] shows that the smoke presence over the Atlantic Ocean south of 20°S is 15–20% of that over South America. The smoke presence is calculated as a summation of the area covered by smoke throughout the 5 month period. Note that because of the larger cloud cover and higher speed of transport over the ocean, the actual fraction of the smoke exiting from South America to the Atlantic can be higher. Chemical analysis of air samples over the Atlantic Ocean during TRACE-A in 1992 confirm the influence of smoke from biomass burning in South America and from Africa [*Gregory et al.*, 1996]. In 1992 there was a vertical separation between the smoke from South America, which was carried aloft by strong convection, and the smoke advected from Africa, which was located below [*Browell et al.*, 1996].

6. Overview of SCAR-B Measurements Program

The main instruments and platforms used in SCAR-B were (1) the NASA ER-2 high-altitude aircraft, which provided multispectral imagery and vertical profiles of clouds and aerosol; these measurements were used to derive fire thermal properties, burn scars, aerosol concentrations, cloud reflectance, cloud microphysics, temperature and spectral reflective properties of the surface, and locations of smoke and cloud layers in the vertical; the ER-2 aircraft conducted 11 flights between August 16 and September 11, 1995; (2) airborne in situ measurements and sampling of aerosol particles, trace gases, and clouds from the University of Washington C-131A research aircraft; measurements included emission factors, the chemical, physical, and optical properties of the aerosol (including the concentration and absorption by black carbon), trace gases, and profiles of the aerosol optical thickness; spectral bidirectional reflectances of various types of surfaces were measured by a scanning, multispectral radiometer to infer hemispherical albedo and to study the correlation of spectral reflectance between the visible and the shortwave-infrared wavelengths [*Tsay et al.*, this issue]. The C-131A aircraft conducted 29 flights in Brazil between August 17 and September 20, 1995 [*Hobbs*, 1996]; (3) airborne in situ measurements and sampling of aerosol particles and selected trace gases by the INPE Bandeirante aircraft; (4) ground-based remote sensing of aerosol from the Aerosol Robotic Network (AERONET). These autonomous Sun photometers provide solar spectral measurements every 15 min that can be used to derive spectral aerosol optical thickness and total precipitable water vapor; once an hour, AERONET provides the spectral sky radiance used to derive aerosol size distributions and estimates of the refractive index of the aerosol and solar absorption by the aerosol; these instruments were operated in Brazil from 1993 to 1995. (5) ground-based in situ measurements at Cuiabá, Alta Floresta, and Natal of the downward spectral radiation field as well as smoke aerosol properties, including size distributions, CCN concentrations, and elemental composition; ground survey measurements of vegetation properties, their spectral and angular reflectance, biomass fuel before and after fires, and fire development; (6) ozonesondes were launched from Cuiabá; and (7) satellite imagery (GOES and AVHRR) were collected to guide the field operations by showing the locations of fires and smoke, for comparisons with the aircraft measurements, and to represent the whole diurnal cycle.

The location of the aircraft on eight representative days of SCAR-B are shown in Plate 4 against a background of the GOES satellite imagery. While the fast-flying ER-2 was able to cover large areas of the cerrado and forest regions on every flight, the C-131A operated successively in several locations obtaining detailed in situ measurements, and shifting its operation center clockwise across the cerrado and Amazon Basin, from Brasília at the beginning of the experiment (Plate 4a) to Cuiabá (Plates 4b through 4e), Porto Velho (Plate 4f through 4h), and eventually to Marabá (see Figure 7) after the ER-2 left Brazil. Figure 7 shows the ground-based stations with the AERONET Sun/sky radiometers and the ground-based sampling of aerosol and trace gases.

6.1. NASA ER-2 Aircraft

Between August 16 and September 11, 1995, the NASA ER-2 aircraft conducted 11 research flights in Brazil as part of the SCAR-B campaign. With its stability, long range (speed of 750 km h^{-1}), and high altitude (20 km), it is an excellent platform to simulate satellite observations of the Earth surface and atmosphere. During SCAR-B the ER-2 was equipped with a cross-track scanning spectrometer (MODIS airborne simulator (MAS)), a hyperspectral imager (airborne visible/infrared imaging spectrometer (AVIRIS)), a downward looking lidar (cloud lidar system (CLS)), and a visible video camera (VIS camera) system.

The MAS is used for measuring reflected solar and emitted thermal radiation in 50 narrowband channels between 550 and 14200 nm [*King et al.*, 1996]. The instrument provides multispectral images of outgoing radiation for the remote sensing of cloud, aerosol, water vapor, and surface properties (see Plate 2). It scans perpendicular to the aircraft flight track with a scan

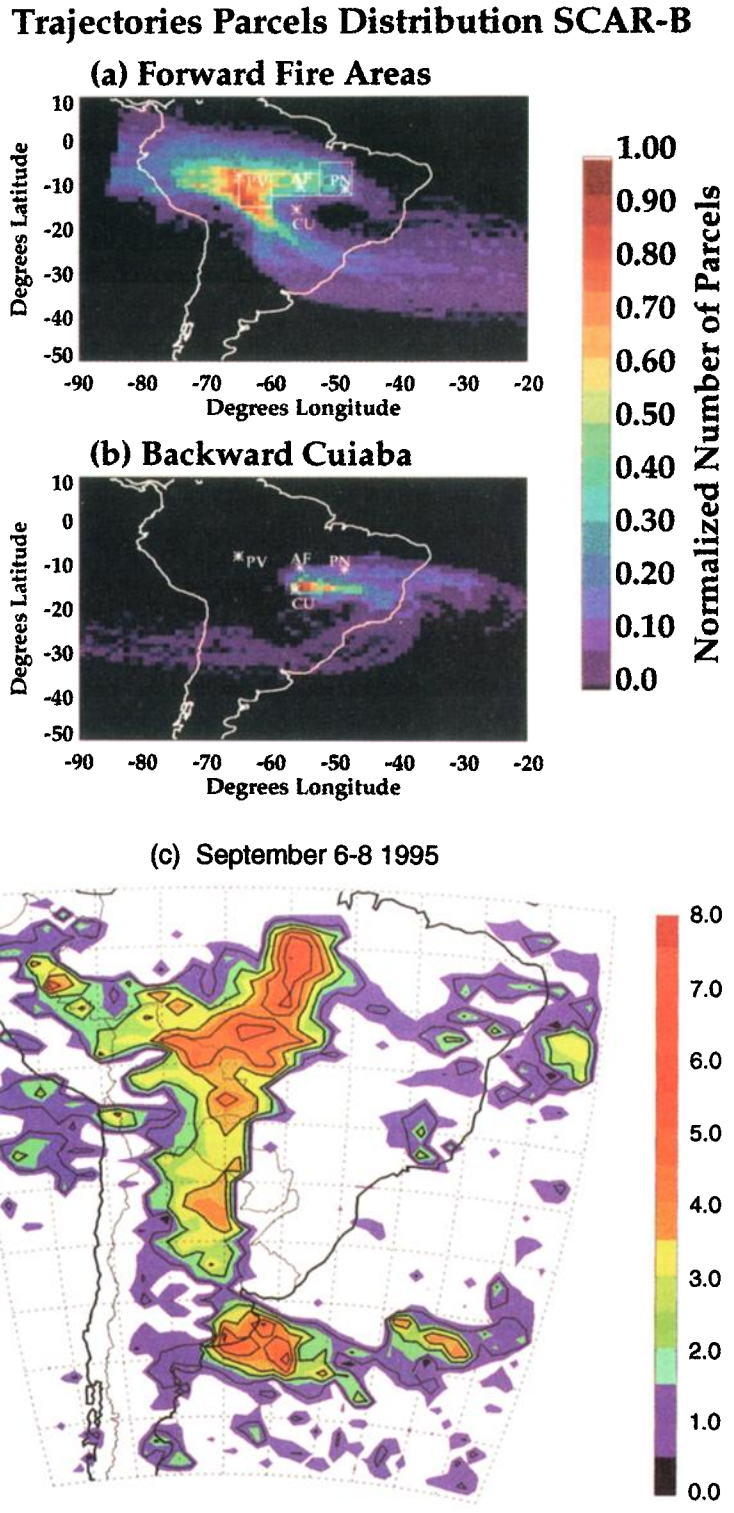

Plate 3. Hourly air parcel locations along (a) 6 day forward trajectories originating from the main biomass burning areas and (b) along 6 day backward trajectories starting from a cluster of points near Cuiabá (16°S, >56°W). Starting levels are ~700 mbar. The trajectory starting points in Plate 3a are distributed according to the main biomass burning areas observed during the experiment from the GOES-8 fire product [*Prins et al.*, this issue]. The trajectories are three-dimensional cinematic calculated from the University of São Paulo model [*Freitas et al.*, 1996] using simulated wind fields with 80 km resolution. (c) Example of GOME data from September 6 to 8, 1995, during the SCAR-B experiment showing the transport of smoke to the Atlantic Ocean. Heavy clouds associated with the transport reduce the ability of satellites to observe it. In this case, 10% of the smoke detected by GOME is over the ocean.

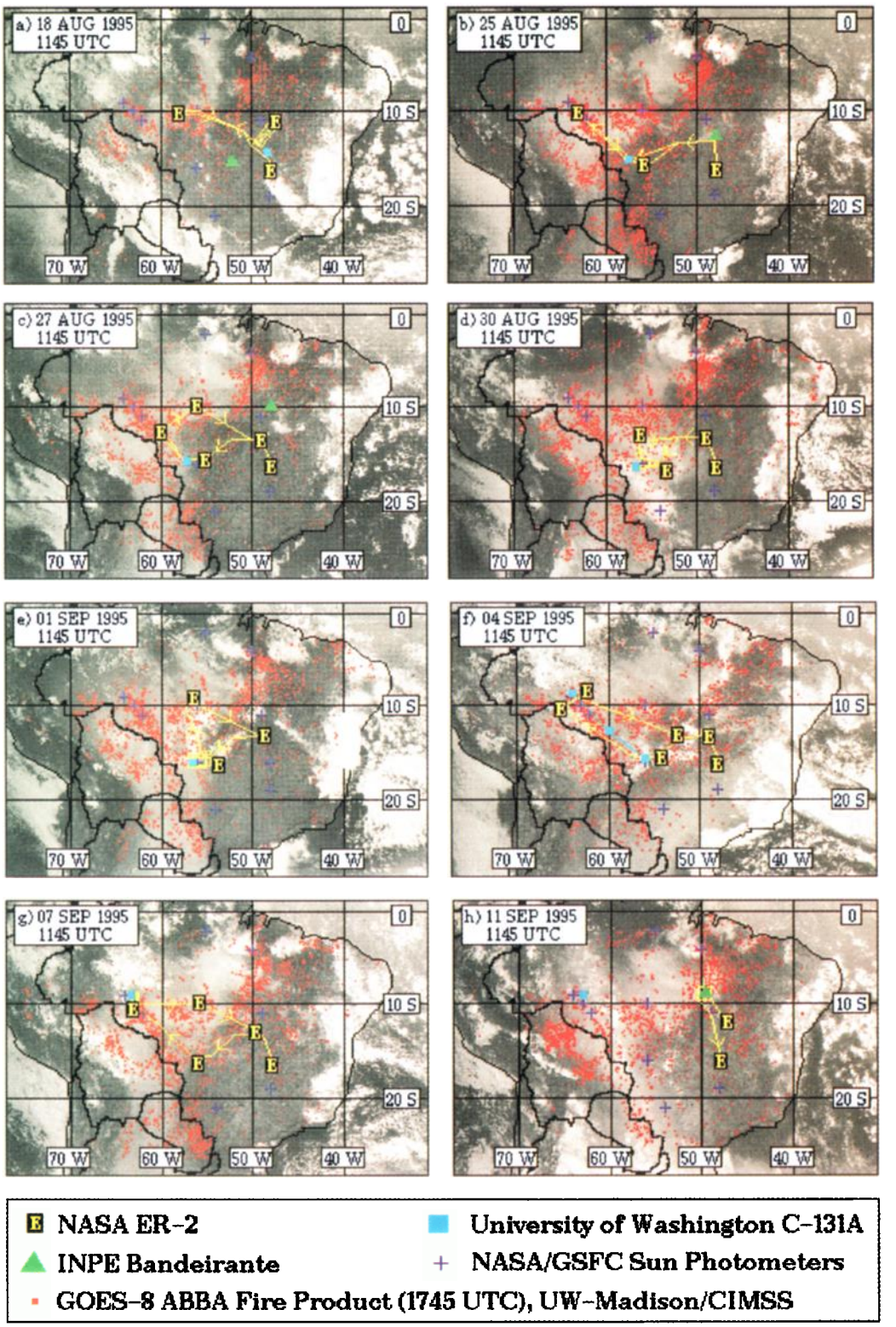

Plate 4. Locations of the SCAR-B aircraft on eight representative days against a background of the GOES satellite images. The GOES data show the distribution of fires (red dots), clouds (white choppy stains), and smoke (light gray smooth features). Ground not covered by smoke appears dark gray. The ER-2 was able to cover cerrado and forest regions on most of the flights; the C-131A operated in several locations moving from Brasília at the beginning of the experiment (a) to Cuiabá (b–e), then to Porto Velho (f–h), and finally to Marabá. The locations of the AERONET Sun/sky radiometers are also shown by the blue crosses.

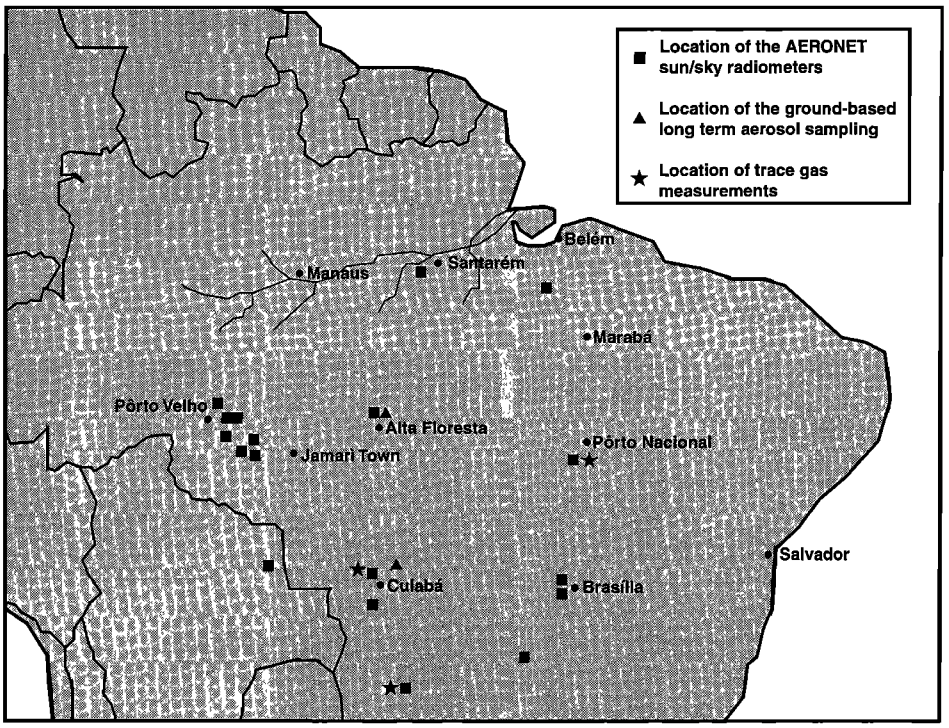

Figure 7. Location of the ground-based measurements. (squares) Location of the AERONET Sun/sky radiometers, (diamonds) location of the ground-based long-term aerosol sampling, (stars) location of trace gas measurements.

angle of ±43° about nadir, spatial resolution of 50 m at nadir, and a 37 km swath width. Radiometric calibration of the shortwave (<2500 nm) channels is obtained by observing laboratory-standard integrating sphere sources on the ground before and after flights; calibration of the infrared channels is performed by viewing two onboard blackbody sources.

The AVIRIS is used to acquire reflected solar radiation in 224 narrow (10 nm width) contiguous spectral bands from 400 to 2500 nm [*Vane et al.*, 1993]. It is a whisk-broom imager, consisting of four spectrometers and linear array detectors, with a spatial resolution of 20 m at nadir and a 10 km swath width. Spectral and radiometric calibrations of the AVIRIS are performed yearly in the laboratory, while in-flight calibrations are conducted before, during, and after each flight season. The recently modified onboard calibrator is expected to achieve 1% stability in radiometric calibration. An AVIRIS image from SCAR-B is also shown in Plate 2.

The CLS is a nadir-viewing monostatic lidar [*Spinhirne et al.*, 1982]. It uses a pulse Nd:YAG laser, transmitting at 532 and 1064 nm with 20 m horizontal resolution. The highest attainable vertical sampling resolution is 7.5 m. This allows construction of detailed cloud and boundary layer aerosol topography and vertical structure (see Plate 2).

During SCAR-B, the ER-2 collected some 69 hours of MAS and CLS data and 11 hours of AVIRIS data. These data sets, taken together, constitute a rich source of information on smoke, clouds, and radiation in Brazil during the biomass burning season of 1995.

6.2. University of Washington Convair C-131A Aircraft

The University of Washington (UW) C-131A research aircraft flew 29 research flights (~90 flight hours) in SCAR-B between August 17 and September 20, 1995. The flights ranged in location from ~16°S to 3°S and from ~64°W to 48°W, which covers the main cerrado and forested areas of Brazil (see examples in Plate 4).

The primary objectives of the C-131A flights were to collect data needed to determine the emission factors of gases and particles, the nature of the gases and particles emitted by various types of fire, the optical and radiative properties of the regional smoke and various types of surfaces, direct and indirect radiative forcing by the smoke, the evolution of smoke properties from local to regional scales, in situ measurements for comparison with remote sensing measurements from the AERONET, the ER-2 aircraft and satellites, and measurements of the spectral bidirectional reflectance function of a wide variety of surfaces in Brazil.

To achieve these goals, the C-131A carried comprehensive instrumentation for measuring the nature and concentrations of gases and aerosols, and surface radiative properties measured by the cloud absorption radiometer (CAR). The CAR, which is mounted on the nose of C-131A, contains 13 narrowband spectral channels between 300 and 2300 nm with a 190° scan aperture (5° before zenith to 5° past nadir) and 1° instantaneous field of view [*King et al.*, 1986]. The bidirectional reflectance is obtained by flying a clockwise circular orbit above the surface, resulting in a ground track approximately 3 km in diameter within about 2 min [*Tsay et al.*, this issue]. A complete listing of the instrumentation on the C-131A and the types of data obtained in SCAR-B are given by *Hobbs* [1996]. The main data collected on the C-131A during SCAR-B were (1) aerosol and gas (NO, NO_2, SO_2, CO, CO_2, O_3, and hydrocarbons) measurements on smoke from 16 cerrado and grass fires and 16 forest and/or slash fires; (2) twenty-three samples for emis-

sion factors for particulates, NO, NO_2, SO_2, CO, CO_2, and total volatile organic compounds (VOCs); (3) four thousand measurements of aerosol size distributions in regional haze and plumes; (4) measurements of volatility of aerosols (at ≤320°C); (5) seventy measurements of humidification factor of aerosols from individual fires and in regional haze; (6) extensive effective black carbon measurements by four techniques (optical extinction cell (OEC), aethelometer, Teflon filters, and thermal-optical; on 26 occasions, simultaneous measurements were obtained using all four techniques; (7) one hundred and 30 measurements of single-scattering albedo of smoke from individual fires and in regional haze; (8) smoke-cloud interaction studies; (9) seven direct aerosol "closure" experiments over ground-based Sun photometers; (10) six coordinated flights with ER-2 aircraft (plus three other "crossings"); (11) four flights during satellite overpasses (AVHRR and Landsat); (12) and seven dedicated surface and smoke reflectivity measurements.

6.3. INPE Bandeirante Aircraft

The INPE Bandeirante aircraft flew from mid-August to mid-September 1995. In the first two weeks it concentrated on measurements of the spatial and vertical variability of trace gases and ozone. In the last two weeks it was equipped with aerosol and trace gas sampling devices and a nephelometer to sample smoke from individual fires and regional smoke haze. The location of the Bandeirante on some representative days is shown in Plate 4.

6.4. AERONET

During SCAR-B the AERONET, consisting of 13 autonomous Sun/sky radiometers, was deployed in the Amazon and cerrado regions of Brazil (see Figure 7). The AERONET provides remote sensing of aerosol loading and properties from the ground, providing validation of aerosol optical properties retrieved from the EOS and ADEOS satellite instrumentation [*Holben et al.*, 1998]. The measurements characterize aerosol properties through continuous long-term monitoring at selected sites around the globe.

AERONET instruments measure the direct solar spectral irradiance and the angular distribution of sky brightness in cloud-free or low-cloud conditions. The data collected by these autonomous instruments, which were preprogrammed and used solar power for energy, were transmitted to satellites and then to NASA GSFC. The data, screened for clouds, were interpreted into spectral aerosol optical thickness, aerosol size distribution, phase function, and for some sites, polarization of sky radiances. The spectral dependence of the optical thickness was represented by the Ångstrom exponent (defined as the slope of the logarithm of optical thickness as a function of logarithm of wavelength between 440 and 870 nm). The measurements represent the whole atmospheric column of aerosol. The total precipitable water vapor was also derived from the differential absorption of water vapor at 940 nm relative to 860 nm. Observations were made at 15 min intervals of the direct Sun in eight spectral wavelengths from 340 to 1020 nm. Measurements of sky radiance (440, 670, 870, and 1020 nm) were made at hourly intervals in an almucantar (a horizontal plane containing the Sun) or principal plane (a vertical plane containing the Sun) scanning mode. In the absence of clouds the almucantar data can be inverted to particle volume size distributions, aerosol optical thickness, and phase function, using a fast radiation transfer inversion code [*Nakajima et al.*, 1996; *Holben et al.*, 1996; *Kaufman and Holben*, 1996].

6.5. Ground-Based Measurements

In addition to the long-term monitoring of trace gases and the production of ozone and smoke aerosol discussed in reference to Figures 1 and 3, measurements were made in SCAR-B of (1) the meteorological conditions in the boundary layer and their effects on the dispersion of pollutants (e.g., mercury) in the atmosphere [*Alvalá et al.*, 1996]; (2) the effects of biomass burning on vegetation and nutrients [*Guild et al.*, this issue; *Castro et al.*, this issue]; (3) the energy budget and distribution of heat in the boundary layer [*Ross and Hobbs*, this issue; T. A. Tarasova et al., unpublished data, 1998], and (4) ground-based measurements of the cloud conditions, nuclei spectrum, and emission factors of individual fires and of the properties of smoke aerosol in regional smoke haze, conducted with the fire atmospheric sampling system (FASS) and compared with the Bandeirante and C-131A aircraft [*Babbitt et al.*, 1996]. Smoke aerosol samples collected on filters were used to determine the elemental compositions and origins of the aerosol [P. Artaxo et al., unpublished data, 1998; *Martins et al.*, this issue (a), (b)].

6.6. Satellite Data

Throughout the 1995 biomass burning season in South America (June–October) the Cooperative Institute for Meteorological Satellite Studies (CIMSS) at the University of Wisconsin-Madison collected 3 hourly, multispectral (visible, 3900, 10,700, and 12,000 nm) Geostationary Operational Environmental Satellite (GOES 8) imagery to monitor diurnal fire activity and smoke coverage and transport [*Prins and Menzel*, 1996]. The study domain included the continent of South America and the South Atlantic Ocean. In support of SCAR-B, half hourly GOES 8 data were collected coinciding with the NASA ER-2 flights. A preliminary version of the CIMSS GOES 8 automated biomass burning algorithm (ABBA version 1.0) was operational during SCAR-B and provided diurnal information on the location of fires and of the extent and transport of smoke throughout the Amazon Basin and over the South Atlantic Ocean (for examples, see Plate 4). GOES 8 imagery, conventional meteorological data, and GOES 8 derived fire and smoke products were also made available daily to SCAR-B scientists, in near-real time as guidance for field program planning.

NOAA 14 advanced very high resolution radiometer (AVHRR) local area coverage (LAC) data were also collected during the experiment and used to estimate the spatial and temporal distribution of fires and smoke during SCAR-B.

7. Overview of SCAR-B Findings

7.1. Fire Properties, Distribution, and Remote Sensing

Fires were detected in SCAR-B using the 20 m resolution AVIRIS and the 50 m resolution MAS on the ER-2 and from GOES (with 4 km resolution) and AVHRR (with 1 km resolution) on satellites. While the ER-2 provided periodic measurements of the fires in many spectral bands and with high spatial resolution (see Plate 2 and *Kaufman et al.* [this issue] and *King et al.* [this issue]), the satellites measured the regional distribution of fires once a day (AVHRR) or several times a day (Plate 4 and GOES [*Prins et al.*, this issue]). The spatial resolution of the images determines the number of fires that

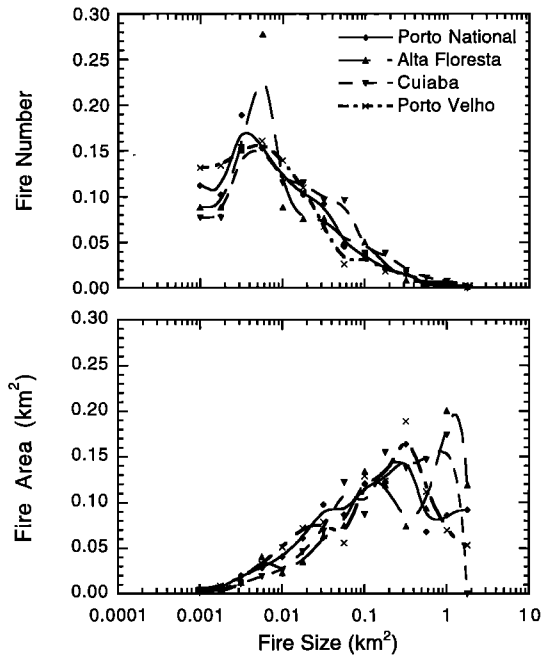

Figure 8. Histograms of the fire size distribution for four locations in Brazil sampled by the MAS instrument on the ER-2 in SCAR-B. Fires are detected using the 3950 nm channel (fire pixel is detected for apparent temperature at 3950 nm > 335 K). (top) The distribution of number of fires as a function of the fire size. (bottom) The distribution weighted by the fire area. All the distributions are normalized to a total probability of 1.0 (data from *Kaufman et al.* [this issue]). Note that the fire size is defined here by the MAS 50 m pixels that have an average apparent temperature at 3950 nm > 335 K.

can be detected, since most fires have a very small flaming or smoldering region, much smaller than 1 km^2. The fire number distribution (Figure 8a) shows maximum concentration of fires of 0.005 km^2 in size. This is the size of the hot region with apparent temperature at 3950 nm greater than 335 K based on MAS observations. Most of these fires cannot be detected by the 1 or 4 km resolution satellite instruments. However, weighting the number of fires by their area (Figure 8b), shows that the bigger fires, which can be observed from satellites, dominate the fire aerial distribution and therefore the rate of biomass burning and emissions. Detailed analysis of the fire detection scheme of the MODIS instrument (1 km resolution) shows that for the four locations studied, MODIS should detect 25% of the fires, but these fires include 60–85% of the thermal radiative energy, a measure that is expected to reflect the rate of biomass burning [*Kaufman et al.*, this issue]. In a previous experiment, we correlated the rate of emission of the fire radiative energy with the rate of emission of smoke into the clean environment of the Northwest United States. In SCAR-B we found a correlation of $r = 0.99$ between the integral of the rate of emission of fire radiative energy and the increase in the size of the burn scar formed by that fire. These measurements were taken in the cerrado region [*Kaufman et al.*, this issue]. Therefore MODIS detection of the thermal energy radiated from the fires should be a good measure of fire intensity and the rate of biomass burning. Only small, nonsystematic differences between the four locations shown in Figure 8 are observed, despite differences in the vegetation cover.

The diurnal evolution of fires was measured in a cerrado region north of Porto National by the ER-2 on September 11. The results plotted in Figure 9 for four flight segments show an increase in the fire density, and an increase in the fire size, as a function of time from noon 1200 (1600 UTC) to 1700. The diurnal cycle is also detected by the GOES 8 fire products that include fire location, ecosystem type, estimates of fire size and temperature at 1145, 1445, 1745, and 2045 UTC each day from June to October 1995 [*Prins et al.*, this issue]. Throughout SCAR-B the GOES 8 ABBA detected a strong diurnal cycle in fire activity, with a peak burning in the middle of the afternoon (1745 UTC), in agreement with the ER-2 data and measurements and observations from the Convair C-131A. Plate 5a provides an example of the fire product at 1745 UTC on August 24, 1995, which was one of the peak burning days during SCAR-B. The figure shows the location of over 4400 fires detected by GOES 8 on this day. The majority of fires were concentrated along the perimeter of the Amazon Basin, in the Brazilian states of Para, Mato Grosso, Amazonas, and Rondonia. There is also considerable activity in Bolivia, Paraguay, and northern Argentina. Large smoke palls were identified in the GOES 8 visible imagery throughout the burning season. During SCAR-B, smoke coverage extended over a large por-

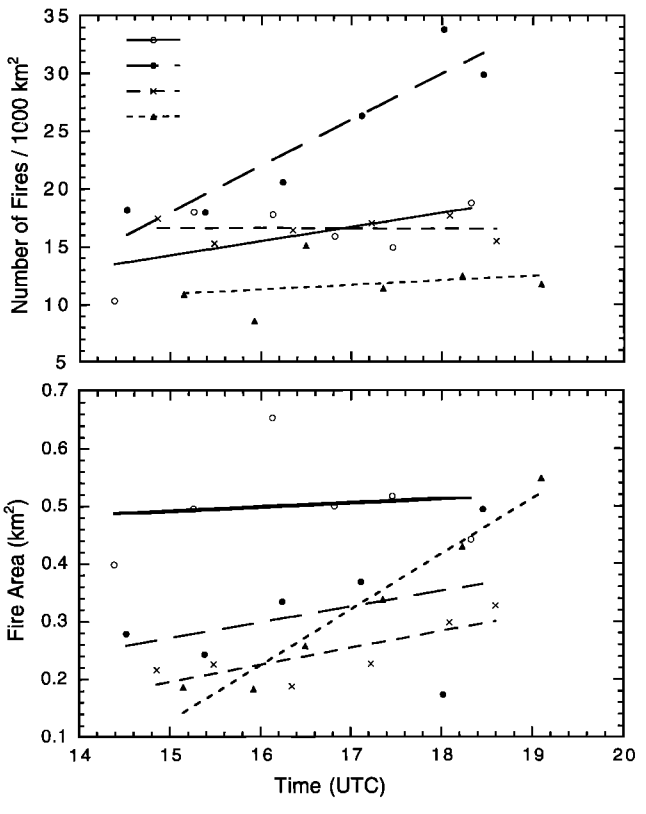

Figure 9. Time dependence of the density of fires (top) and the average area of fires (bottom) measured by the MAS instrument on the ER-2 on September 11, 1995, over a cerrado region north of Porto National, Brazil. The ER-2 returned 6 times to the same four legs of a square box, bounded by latitude lines of 8.2°S and 9.5°S and longitude lines 49°W and 50.5°W. The local time was 4 hours less than UTC, therefore the six repeated measurements occurred from noon until 1700 LT. The different symbols correspond to four legs of a box flown by the ER-2. The straight lines are least square fits to the data on each leg.

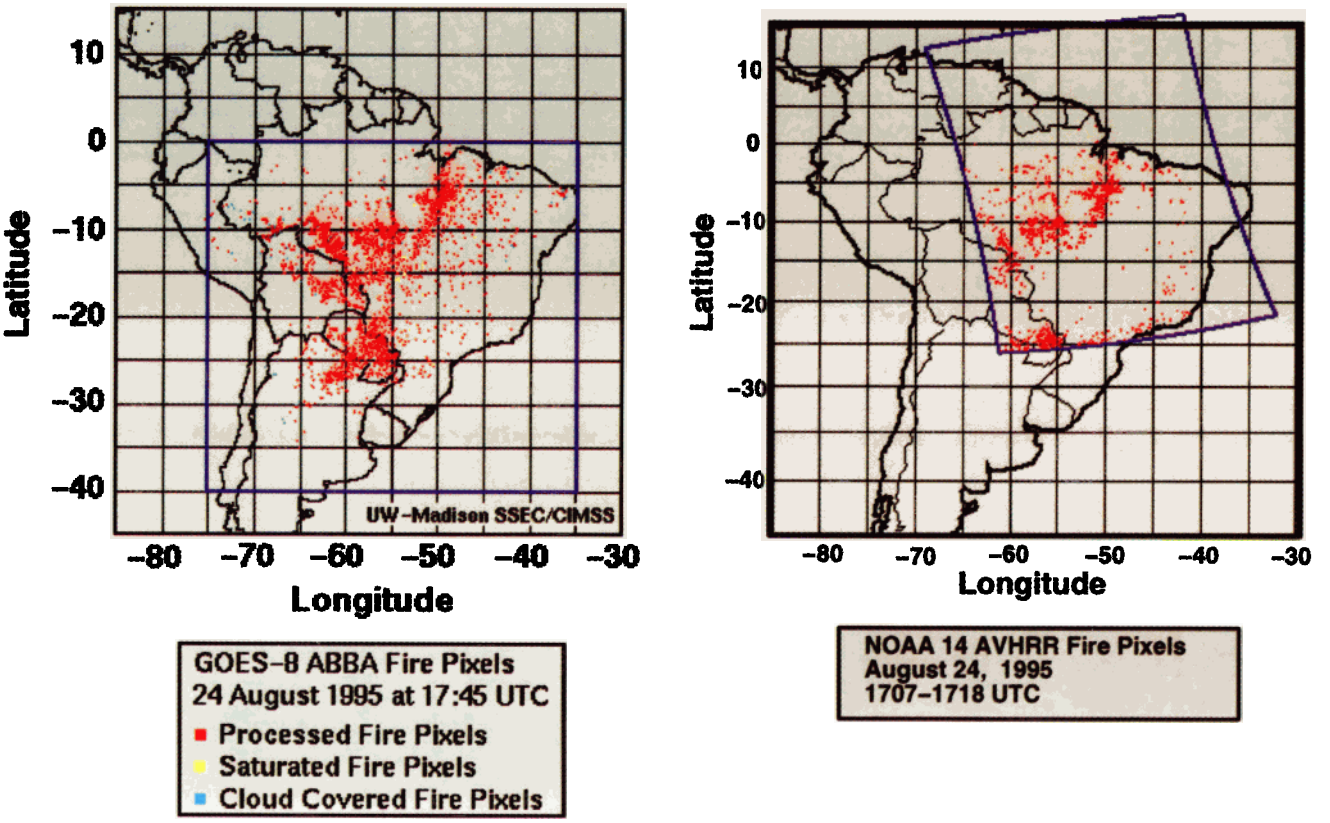

Plate 5. Example of fire detection from satellites by GOES-8 (4 km resolution 3950 nm channel) and AVHRR (1 km resolution 3750 nm channel). (a) The GOES-8 fire product at 1745 UTC on August 24, 1995, one of the peak burning days during SCAR-B, showing the locations of over 4400 fires detected with the GOES-8 ABBA algorithm. The red markers indicate fires that were processed by the GOES-8 ABBA providing estimates of subpixel fire size and temperature; yellow indicates saturated fire pixels; and blue represents cloud-covered fire pixels. (b) NOAA-14 advanced very high resolution radiometer (AVHRR) local area coverage (LAC). The red dots indicate the fire pixels, and the region enclosed in blue is the area covered by the NOAA-14 AVHRR for this day between 1707 and 1718 UTC.

tion of the continent east of the Andes Mountains for a period of several weeks, with transport over the Atlantic Ocean on many days [*Prins et al.*, this issue].

Fire pixels were also identified from the NOAA 14 AVHRR 1 km resolution data using a series of spectral conditions, and the results are categorized for major ecosystems within South America. An example of the AVHRR-derived fire pixels for 24, August 1995, is shown in Plate 5b. The red dots indicate the fire pixels detected in the enclosed area covered by the NOAA 14 AVHRR for this day between 1707 and 1718 UTC. The fire activity is mainly in the states of Rondonia, Para, Amazonas, and Mato Grosso. A total of 3150 fire pixels were detected from this image, with large smoke palls extending from Rondonia and Mato Grosso into Bolivia, Paraguay, and Argentina. A comparison to the GOES 8 fire detection shows similar fire patterns along the perimeter of the Amazon in the states of Maranhao, Tocantins, Para, Mato Grosso, Rondonia, and Amazonas, although the GOES 8 ABBA shows considerably more fire activity in Rondonia. The ABBA also shows more fires in the cerrado/grassland regions of eastern Brazil and in Paraguay. The AVHRR fire product shows more fire activity associated with deforestation along the Amazon River and along the Atlantic Coast in southeast Brazil. The difference in fire counts for NOAA 14 AVHRR (3150) and GOES 8 (4417) is due, in part, to a difference in study domains as depicted in the blue outlines in Plate 5; it also reflects the difference in observing time, sensing capabilities, and fire detection algorithms. Although the NOAA 14 and GOES 8 observing times are separated by less than 1 hour in this example, the strong diurnal cycle in burning may result in significant changes within this time period.

7.2. Emission Factors

The modified combustion efficiency (MCE) and the emission factors (EF in g kg^{-1}) of trace gases and smoke particles from individual fires were measured by the FASS system from a ground-based station in Porto Velho and from the Bandeirante aircraft [*Babbitt et al.*, 1996]. They were also measured aboard the C-131A aircraft [*Ferek et al.*, this issue; *Reid and Hobbs*, this issue]. The modified combustion efficiency is defined as

$$\mathrm{MCE} = \frac{[\mathrm{CO_2}]}{[\mathrm{CO}] + [\mathrm{CO_2}]} \quad (1)$$

The main results are summarized in Table 2. Detailed results are given in the above referenced papers in this special issue. While the FASS measurements concentrated on a few fires and on comparisons between ground-based and aircraft measurements, the measurements made aboard the UW C-131A aircraft were for a wide variety of vegetation (grass, cerrado, forest) and in various regions of Brazil.

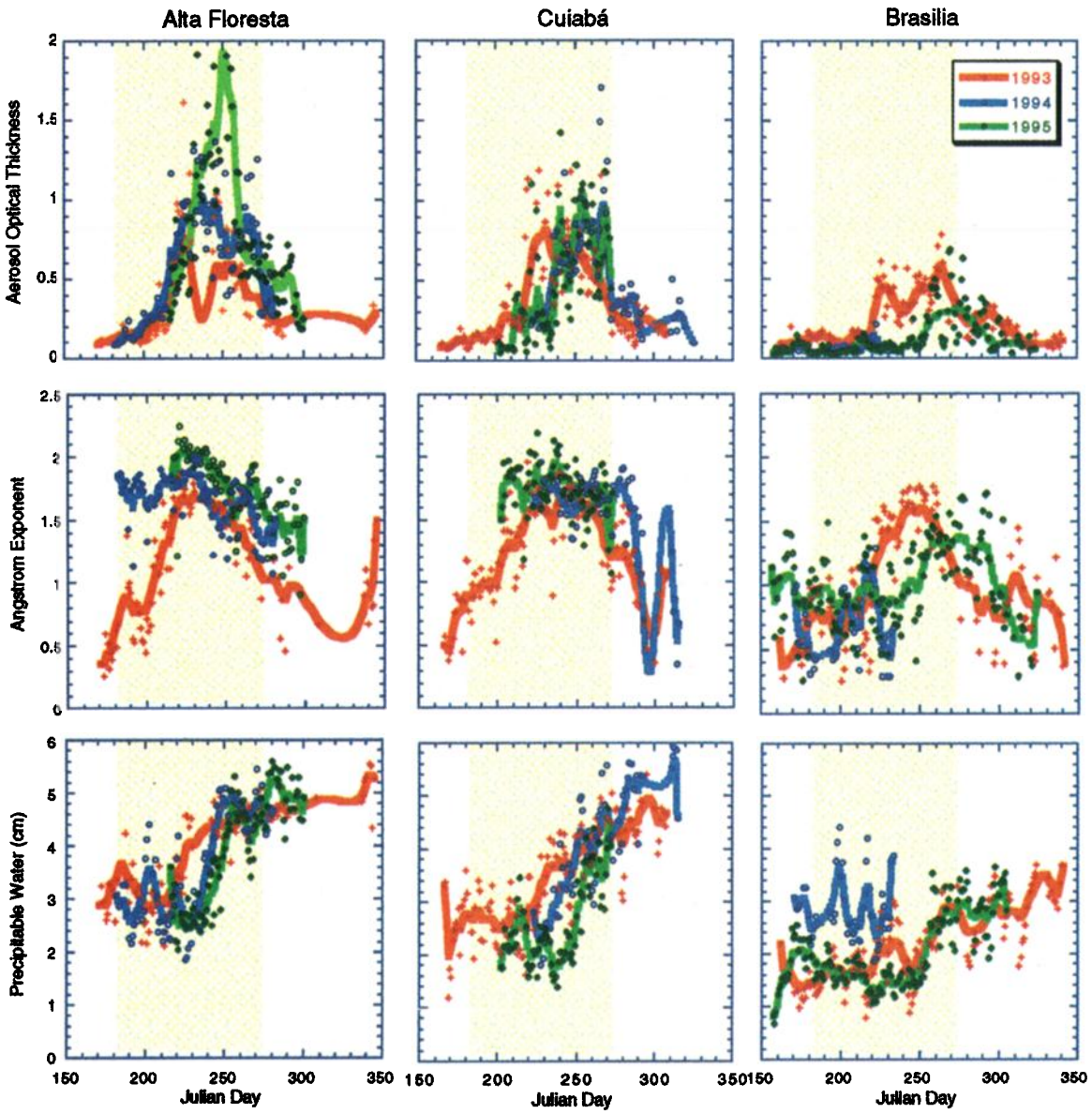

Plate 6. Measurements from the AERONET Sun/sky scanning spectral radiometers at three SCAR-B sites for 1993–1995. (top row) Aerosol optical thickness at 670 nm. (middle row) Ångstrom exponent (slope of the logarithm of the optical thickness as a function of the logarithm of the wavelength between 440 and 870 nm). Higher values of the Ångstrom exponent correspond to larger contributions of smoke particles. Because of a failure of the 870 nm filter at Alta Floresta in 1994, the Ångstrom exponent for that year was based on 440 and 670 nm combination. (bottom row) Total precipitable water vapor, derived from the differential absorption of water vapor at 940 nm relative to 860 nm. The dots are daily averages approximately between 0900 and 1500 LST. A smooth curve is drawn through the data for each year. The yellow band in each figure shows the burning season (July 1 to September 30).

In agreement with ground-based measurements in Brazil and Africa [*Ward et al.*, 1992, 1996] the C-131A measurements showed hydrocarbon (HC) emissions to be associated with smoldering combustion (i.e., low temperature, inefficient combustion). The concentration of total nonmethane hydrocarbons (NMHC), as well as individual HC, correlated better with CO than with CO_2, regardless of vegetation type, in agreement with *Lobart et al.* [1991]. For NMHC versus CO the correlation coefficient (r) was generally $r > 0.90$, whereas for NMHC versus CO_2, the correlation was generally $r < 0.75$. Methane behaved similarly to the NMHC. The CO concentration is an indicator of the combustion inefficiency given by (1-MCE) in Table 2.

Halocarbons exhibited a complex emission pattern. Only methyl bromide, methyl chloride, and methyl iodide appeared to derive unambiguously from biomass burning, and they correlated reasonably well with the MCE (see Table 2). The negative correlation indicates more efficient emissions in the smoldering stage, which is identified with a lower MCE.

SO_2 and NO_x behaved opposite to that of the HC, in that their emission factors increased with increasing combustion efficiency. Thus the emissions of these gases were associated

Table 2. Summary of Correlations Between Modified Combustion Efficiency (MCE = $[CO_2]/[CO_2] + [CO]$) and Emission Factors (EF in g/kg) of Trace Gases and Particles and Particles Sizes, Measured From Ground by FASS System [*Babbitt et al.*, 1996] and From C-131A Aircraft [*Ferek et al.*, this issue; *Reid and Hobbs*, this issue].

Parameter	Correlation Coefficient (r) With MCE	Biomass Type	EF/(1 − MCE)
	FASS Measurements From Ground and From Bandeirante [Babbitt et al., 1996]		
Methane	−0.92	pasture	~70
Methane	−0.95 to −0.98	primary forest	84
NMHC	−0.28	pasture	27
NMHC	−0.87 to −0.91	primary forest	34 ± 9
Smoke fine particles ($d < 2.5$ μm)	−0.26	pasture	57
Smoke fine particles ($d < 2.5$ μm)	−0.44	primary forest	
	−0.72	ground-based measurements	13
		airborne measurements	40
	C-131A Measurements, [Ferek et al., this issue]		
NMHC	−0.70	primary forest, cerrado, and pasture	10
Methyl bromide	−0.89 or −0.66	primary forest, cerrado, and pasture	1.16
Methyl chloride	−0.70	primary forest, cerrado, and pasture	
Methyl iodide	−0.81	primary forest, cerrado, and pasture	
Smoke fine particles ($d < 3.5$ μm)	−0.49	primary forest, cerrado, and pasture	10
SO_2	0.36	primary forest, cerrado, and pasture; emission ratio of 0.02% per volume	
NO_x	0.39	primary forest, cerrado, and pasture; emission ratio of 0.2% per volume	

Parameter	Correlation Coefficient (r) With MCE	Properties
	Reid and Hobbs [this issue]	
Count median diameter (CMD) for young smoke from forest fires	0.83	CMD = 0.10 μm for MCE = 0.84 CMD = 0.14 μm for MCE = 0.98
Particle volume median diameter (VMD)	−0.44	VMD for young smoke ~0.26 μm, VMD for older smoke in regional hazes ranged from 0.28 to 0.35 μm
Black carbon	no correlation	about 6–8% of the emitted particle mass

more with flaming combustion. The NO_x to CO_2 emission ratio measured on the C-131A was 0.2%. This is just under the range of 0.3–0.6% measured in Africa [*Lacaux et al.*, 1996]. Higher NO_x emission rates in Africa can be expected due to the higher combustion efficiencies (95%) of these fires. *Lacaux et al.* [1996] found that the NO_x emissions are also correlated with the nitrogen concentrations in the burned biomass.

Measurements from the C-131A aircraft showed that the particle count median diameter (CMD) was strongly and positively correlated with the MCE. For young smoke from forest fires, the CMD varied from 0.10 μm for smoldering condition (MCE = 0.84) to 0.14 μm for flaming condition (MCE = 0.98). The particle volume median diameter (VMD) decreased slightly with increasing MCE. The VMD correlated well with the emission factors for particles and unsaturated hydrocarbons. The mean value of the VMD for young smoke was ~0.26 μm, and for older smoke in regional hazes, it ranged from 0.28 to 0.35 μm [*Reid and Hobbs*, this issue; *Reid et al.*, this issue]. The effective emitted amount of black carbon (BC), derived from absorption measurements, overall comprised about 6–8% of the emitted particle mass and appeared to vary randomly from fire to fire. Details are given by *Ferek et al.* [this issue]. Discussion of the relationship between BC and smoke absorption is given in section 7.4 below.

7.3. Trace Gas Measurements

Atmospheric trace gases were measured on the INPE Bandeirante aircraft, a Brazilian research aircraft described in detail by *Kirchhoff and Alvalá* [1996]. The gases measured were (1) CO_2 by an IR nondispersive technique, (2) O_3 by a UV photometer, and (3) CH_4, N_2O and CO collected by grab samples [*Alvalá and Kirchhoff*, this issue]. A composite of the CO_2 results is shown in Figure 10. These results show a considerable dispersion of the data around an average CO_2 value of 8 ppmv above the background conditions of 352 ppmv. Despite the fact that direct biomass burning plumes were avoided in this survey, clearly biomass burning affected the regional values of CO_2. Note the repeatability of the different measurements. The enhanced CO_2 does not vary significantly with altitude under the strong inversion.

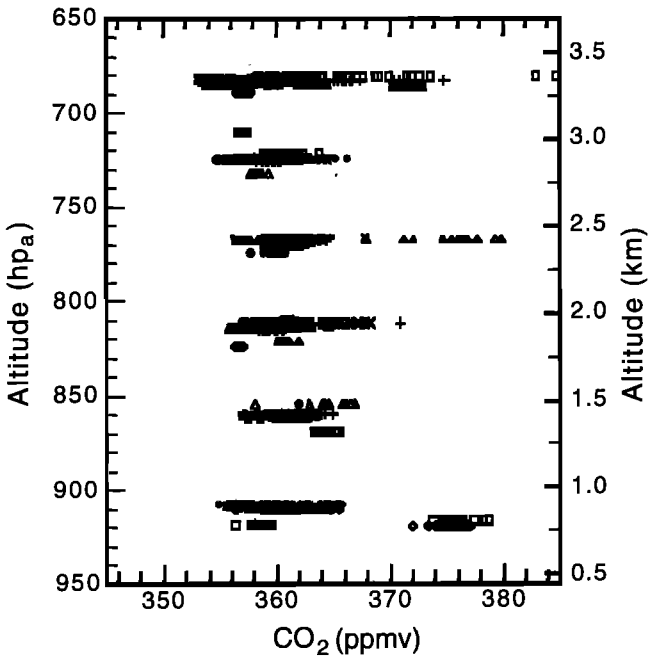

Figure 10. Vertical profiles of CO_2. Altitudes are given in hPa on the left and in kilometers on the right. Different symbols are used for different flights/locations. The spread of CO_2 mixing ratios indicates the spatial variability of its concentration. The lowest values correspond to the background CO_2 concentrations at different altitudes.

Ozonesondes were launched from Cuiabá, and a total of 25 vertical profiles of ozone, relative humidity, and temperature were obtained during SCAR-B. The tropospheric ozone concentration appeared enriched during the period. Average values ranged from 40 to 90 ppbv; wet season values are typically around 15 ppbv. A correlation between tropospheric ozone concentration and aerosol optical thickness in Cuiabá (e.g., Figure 11) was observed with two patterns that reflect different air circulations [*Longo et al.*, 1998]. The increase in ozone concentration with aerosol optical thickness is an additional indication of the direct effect of biomass burning on ozone concentration.

7.4. Aerosol Properties and Evolution

One of the main objectives of SCAR-B was to obtain comprehensive measurements of the properties of the smoke aerosol. Remote sensing techniques from ground, aircraft, and satellites were used in conjunction with in situ measurements. Long-term monitoring of aerosol properties was conducted in Cuiabá and Alta Floresta, as indicated in Figure 3. Aerosol properties and loading were also measured in situ from the C-131A and Bandeirante aircraft, as well as from a ground-based site in Cuiabá. They were also monitored by remote sensing from the ground-based Sun/sky radiometer (AERONET) sites and by spaceborne remote sensors. The C-131A aircraft also provided comprehensive measurements of the optical and radiative properties of the smoke particles.

7.4.1. Aerosol retrieval from AERONET. The AERONET sites at Brasília, Cuiabá, and Alta Floresta have been instrumented since 1993 for the duration of the dry season, which typically begins around 1 June (Julian day 152) and lasts through 1 November (day 305). The data are used here to describe the smoke evolution during SCAR-B and to compare the SCAR-B measurements with previous years. These measurements are not described elsewhere in this issue.

In Plate 6 the evolution of aerosol optical thickness at 670 nm, Ångstrom exponent, and total precipitable water vapor are shown for these three sites for the three years of observations. The Ångstrom exponent provides a crude measure of the aerosol size distribution. A zero value indicates mainly large particles (e.g., the presence of desert dust); a value of 2 indicates dominance by small particles (e.g., fine-mode smoke particles). Brasília, Cuiabá, and Alta Floresta represent three diverse measurement locations. Brasília, a high-elevation cerrado region, is characterized by a significant conversion of natural vegetation cover to agriculture. Cuiabá, a low-elevation cerrado region located in an agricultural area, is within 500 km of forest-to-agricultural conversion to the north and the Pantanal to the South (both noted for dry season burning). Alta Floresta is located in a region of very active forest conversion to agriculture. The AERONET measurements at this site show considerable variation from year to year in the smoke concentrations at midseason and at the onset and termination of the burning season [*Holben et al.*, 1996]. All sites exhibit an aerosol optical thickness in the preburning season of 0.10 to 0.15 (higher in 1993 due to the presence of stratospheric aerosol from the eruption of Mount Pinatubo in the Philippines). This stratospheric aerosol also lowered the Ångstrom exponent in 1993, mainly before and after the burning season.

For all three years shown in Plate 6, the interannual variability of the burning is within the envelope of meteorological variables that broadly control the burning season (e.g., the length of drying time and the onset of rains). The precipitable water and aerosol optical thickness records clearly show that the majority of emissions occur when the water vapor content of the atmosphere is increasing. This can potentially affect the aerosol optical properties during the burning season, although due to the small humidification factors of the smoke aerosol found in SCAR-B [*Kotchenruther and Hobbs*, this issue], we do not anticipate large effects of humidity on particle size. For 1995 the water vapor content of the atmosphere was lower for longer periods than in previous years, which likely accounts for a more intense late burning season and an associated higher aerosol optical thickness. The optical thickness was higher in the forest regions (Alta Floresta) than in the cerrado regions near Brasília. In Cuiabá, smoke was transported part of the

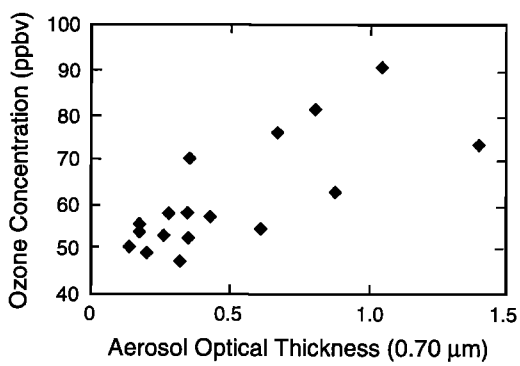

Figure 11. Average ozone concentration (from 1000 to 500 mbar) as function of the aerosol optical thickness, AOT (0.70 μm channel). A split pattern is observed due to a change in the air circulation pattern.

time from forest conversion areas to the north of the city, increasing the optical thickness.

The burning season in Brasília was relatively weak in 1995, starting thirty days later than in 1993 and terminating around 30 October (day 310). The Ångstrom exponent mirrors the optical thickness, with an increase from 0.8 to 1.4 from preburning to the burning season. Precipitable water increased from 1.3 cm (day 240) to 3 cm (day 260), in both 1993 and 1995. For the first part of the dry season, 1994 shows elevated precipitable water compared to the other two years.

Cuiabá shows twice as much smoke (optical thickness $\tau_a \sim 0.9$) as Brasília, due to transport from the north. Here also the duration of the burning season was shorter in 1995 than in 1993. The Ångstrom exponent in the burning season ranged from 1.6 to 1.8, dropping to 0.9 before and after the burning season. Precipitable water varied from 2 to 5 cm within 60 days of the most intense part of the burning season. In 1995 the increase in precipitable water began 30 days later than in 1993. All years reached a wet season value for the precipitable water of 4.6 cm. The effect of a more intense dry season in 1995, and the higher rate of deforestation, is marginally apparent in higher late season optical thickness values in 1995 as compared to 1993.

Alta Floresta has a significantly higher optical thickness than the cerrado sites, mainly in 1995, due to its proximity to the burning areas. The Ångstrom exponent is accordingly higher (~2). The onset and duration of the burning season is approximately the same for all years, and similar to Cuiabá and Brasília. The precipitable water vapor increased from 2.0 to 5.5 cm in each of the three years but more gradually in 1993 than for the other years.

7.4.2. Aerosol measurements aboard the C-131A. In situ measurements aboard the C-131A aircraft provided detailed information on the composition, size distributions, shapes, humidification factors, and optical properties of aerosols in the smoke from various types of biomass fires and in the aged smoke that dominated regional hazes in the study areas.

7.4.2.1. Composition: For smoke from individual fires, inorganic ions and black carbon (BC) together accounted for only ~15–20% of the mass of the smoke aerosol; the remaining mass is surmised to have been organics. The corresponding percentage for aerosols in regional hazes dominated by smoke was ~20–25% [*Reid and Hobbs*, this issue; *Reid et al.*, this issue (a), (b)]. Biomass burning aerosol particles dominated the mass loading, but three other aerosol components were also observed: soil dust particles, natural biogenic particles, and NaCl particles. Individual particle analysis as well as multivariate statistical techniques showed similar type of particles [*Artaxo et al.*, this issue].

7.4.2.2. Growth: As the smoke particles aged, the CMD (count median diameter) increased from about 0.10–0.13 μm diameter in smoke plumes to 0.11–0.18 μm diameter in regional hazes. This growth appeared to occur equally between the first few hours following emission and the next few days. The Ångstrom exponent (for the wavelength range 550–700 nm) was 2.5–2.9 for smoke plumes and 1.8–2.3 for regional hazes (similar to the AERONET results), which supports a significant increase in particle size with aging. The growth with age of the aerosols appeared to depend equally on the availability of condensates relative to the particle concentrations and on coagulation. Condensation was mainly onto existing particles. Changes in the contributions of BC, potassium, and CO (all conservative traces) to the mass of aerosols indicate that aerosol mass increased by ~20–50% during aging. About 75% of this growth was due to the condensation of organic species and ~25% from ammonium, sulfate, and nitrate.

The growth of the particles with age had a large effect on their optical properties. The hemispheric backscatter fraction of the particles decreased from ~0.18 to 0.12, and the single-scattering albedo of the particles at 550 nm increased from ~0.79 for young smoke to ~0.85 in regional hazes [*Reid and Hobbs*, this issue; *Reid et al.*, this issue (a)].

7.4.2.3. Shapes: Since Mie calculations apply strictly only to spherical particles, it is important to obtain information on the shapes of the aerosol particles produced by biomass burning. The paper by *Martins et al.* [this issue (b)] provides such information from electron microscopy of individual particles and from an instrument aboard the C-131A aircraft that provided continuous measurements of the effect of the asymmetry of the particles on the light-scattering coefficient. The results indicate that for optical calculations the smoke particles in regional hazes dominated by smoke in Brazil can be reasonably approximated as spherical.

7.4.2.4. Humidification factors (HFs): *Kotchenruther and Hobbs* [this issue] define the HF as the light-scattering coefficient for particles at 80% relative humidity (RH) divided by the light-scattering of dry particles (40% RH). For smoke in Brazil, 80% of the measured HF were in the range 1.05–1.35 (compared to a mean value of 2.30 ± 0.24 for urban/industrial aerosol on the U.S. East Coast [*Kotchenruther et al.*, 1998]). These relatively low values for the HF have an important effect on direct radiative forcing by smoke [*Hobbs et al.*, 1997; *Kotchenruther and Hobbs*, this issue]. Similar values were found in the TRACE-A experiment for smoke both from Brazil and from South Africa (Table 3) [*Anderson et al.*, 1996]. But a mixture of smoke with industrial sulfate aerosol such as in South Africa [*Maenhaut et al.*, 1996] may increase the hygroscopicity. In the recent Indonesian biomass fires, low refractive indexes were derived [*von Hoyningen-Huene et al.*, 1998] indicating, indirectly, a higher hygroscopicity of the smoke. In this case, high-sulfate concentrations were measured due to underground coal that was burning together with the biomass, or due to industrial emissions (T. Nakajima, personal communication, 1998).

7.4.2.5. Measurements of black carbon (BC) and shortwave absorption by smoke aerosol: BC is the major component of the atmospheric aerosol that absorbs solar radiation, and biomass burning is an important source of BC, although other components of the aerosol can also absorb sunlight. Unfortunately, measurements of the concentrations of BC in the atmosphere and measurements of absorption are subject to many uncertainties. In SCAR-B, five different measurement techniques were used to measure BC aboard the C-131A. Two additional methods were applied using ground-based remote sensing. The results of these comparisons are described by *Reid et al.* [this issue]. In brief the correlation between the concentrations of BC derived from thermal techniques and optical absorption was poor. This could be due to uncertainties in some of the measurements, from the presence of absorbing "gray" organic material [*Novakov et al.*, 1997], or from mixtures of BC with nonabsorbing materials. The various values derived for the light absorption coefficient (σ_a) agreed to within ±20%. The in situ measurements show that the single-scattering albedo (ω_0) of smoke varied from 0.35 for plumes from vigorous flaming grass fires to 0.9 for smoldering slash. The uncertainty in the single-scattering albedo for the plume

Table 3. Smoke Aerosol Dynamic Model Based on *Remer et al.* [this issue] Describing Variability of Regional Smoke Ambient Aerosol Optical and Physical Parameters for Total Vertical Column As Function of Aerosol Loading (Given by Optical Thickness)

Parameter	Fine Particle Mode ($d < 2$ μm)	Coarse Particle Mode ($d > 2$ μm)	Remark/Reference
Particle volume ($\mu m^3\ \mu m^{-2}$)	0.3τ ($\pm 0.01\tau$)	0.8τ (±large)	*Remer et al.* [this issue]
r_m = volume mode radius μm)	0.135 ± 0.02	10 (±large)	*Remer et al.* [this issue]
	0.13–0.17		*Reid et al.* [this issue]
	0.15 (SCAR-B in situ)		*Artaxo et al.* [this issue]
	0.13–0.15 (TRACE-A, SAFARI)		*Anderson et al.* [1996]
			Le Canut et al. [1996]
σ = standard deviation (s.d.) of ln σ_{gv}, where σ_{gv} = geometric s.d. of particle volume distribution	0.60 ± 0.05	1.2 ± 0.3	*Remer et al.* [this issue]
	0.4–0.6		SCAR-B in situ [*Ross and Hobbs*, this issue]

Parameter	Values of Wavelength λ	Remarks/Reference
Single-scattering albedo (ω_0)	λ470–670: 0.9	*Remer et al.* [this issue]
		Kaufman et al. [1992]
	λ450: 0.86, λ550: 0.83, λ700: 0.71 (±0.04)	*Hobbs et al.* [1997]
		Reid et al. [this issue (a)]
	λ440: 0.80, λ670: 0.87, λ870: 0.88 (±0.06)	*Dubovik et al.* [this issue]
	broadband (Indonesian 1997 fires) 0.90–0.91	*von Hoyningen-Huene et al.* [1998]
	0.90–0.92 model for South America and Africa	*Liousse et al.* [1996]
Real part of refractive index	1.52–1.60	*Yamasoe et al.* [this issue]
	1.37–1.55—Indonesian 1997 fires	*von Hoyningen-Huene et al.* [1998]
Asymmetry parameter (g)	λ440: 0.65, λ670: 0.,57, λ870: 0.49, λ1020: 0.45 (±0.06)	*Remer et al.* [this issue]
Upscatter fraction ($\bar{\beta}$)	λ440: 0.24, λ670: 0.27, λ870: 0.31, λ1020: 0.32 (±0.02)	*Remer et al.* [this issue]
	λ450: 0.24, λ550: 0.25, λ700: 0.28 (±0.20)	*Hobbs et al.* [1997], *Reid et al.* [this issue (a)]
CCN/τ	130 ± 40 (μm^{-2}) at supersaturation S = 0.3%	*Remer et al.* [this issue]
	170 ± 80 (μm^{-2}) at supersaturation S = 1%	
Mass scattering efficiency ($m^2\ g^{-1}$)	λ440: 6.6, λ670: 3.2, λ870: 2.1, λ1020: 1.6	*Remer et al.* [this issue]
	λ450: 4.1–4.9, λ550: 2.9–4.1, λ700: 1.6–2.4 λ600: 4.2	*Hobbs et al.* [1997], *Reid et al.* [this issue (a)], *Anderson et al.* [1996]
Mass absorption efficiency ($m^2\ g^{-1}$)	λ550: 0.6–0.9	*Reid et al.* [this issue (a)]
Humidification factor at 80% relative humidity	λ450–λ700: 1.05–1.35	*Kotchenruther and Hobbs* [1998]
	1.37 ± 0.14 in Brazil, TRACE-A	*Anderson et al.* [1996]
	1.14 ± 0.02 in South Africa, TRACE-A	

The optical thickness τ is measured at 670 nm. The wavelengths are noted e.g., λ44 means λ = 440 nm). Comparisons to SCAR-B and non-SCAR-B in situ measurements are given based on *Hobbs et al.* [1997] and *Reid et al.* [1998a, b]; these measurements are for dry aerosol, Therefore small differences due to humidity are expected.

data was ±0.03. For regional hazes, ω_0 varied between 0.8 and 0.9, with an uncertainty of ±0.04 to ±0.08 for the different optical methods. Ground-based remote sensing of ω_0 using irradiance data gave values of 0.8 to 0.92, decreasing with wavelength, similar to the in situ measurements [*Eck et al.*, this issue]. Values of ω_0 derived from sky radiances [*Dubovik et al.*, this issue] indicate that ω_0 may increase with wavelength from 0.80 at λ = 440 nm to 0.88 at 870 nm. Therefore although these methods agree on an average single-scattering albedo in the visible wavelengths (λ = 440–660 nm) of 0.86 ± 0.05, they disagree at longer wavelengths. The differences could be due to measurement techniques and differences in the smoke composition.

Mass absorption efficiencies for black carbon (α_{abc}) in smoke particles were derived using the thermal evolution [*Cachier et al.*, 1989] and optical absorption techniques [*Reid et al.*, this issue]. Values of α_{abc} ranged from 5 to 58 $m^2\ g^{-1}$ (see Figure 12). The variability of α_{abc} was modeled for internal (layered sphere and closely packed clusters) and external mixing between BC and nonabsorbing materials. The calculated values of α_{abc} were between 5 and 25 $m^2\ g^{-1}$ for the measured size distributions [*Martins et al.*, this issue (a)]. Measured values of α_{abc} higher than 25 $m^2\ g^{-1}$ were attributed to possible artifacts in the measurements by the thermal technique due to a catalytic effect on BC particles caused by certain chemical compounds. *Novakov et al.* [1995] suggested that K may have a catalytic effect on BC, lowering its volatilization temperature. On the basis of this assumption, a threshold value of K/BC = 0.78 was established for which most of the α_{abc} measurements could be explained by the assumed models. Figure 12 shows the measured values of α_{abc} compared to the modeled values. On average, for samples with K/BC < 0.78, the value of α_{abc} is 12.1 ± 4.0 $m^2\ g^{-1}$ [*Martins et al.*, this issue (a)].

7.4.2.6. Closure studies: Data for aerosol column closure studies (i.e., consistency tests) were obtained by flying the C-131A in vertical profiles over AERONET Sun photometers in Brazil under conditions dominated by regional smoke. From the airborne in situ measurements of the aerosol properties,

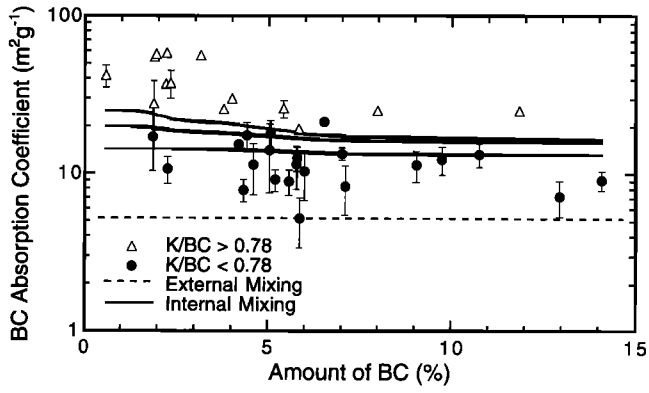

Figure 12. Measured and modeled black carbon (BC) absorption efficiency (α_{abc}) at $\lambda = 550$ nm versus the amount of BC in the sample determined from thermal analysis. Solid lines represent the modeled α_{abc} for three measured particle size distributions using a layered sphere model with a BC core and a nonabsorbing shell. The dashed line is the asymptotic limit for α_{abc} assuming external mixing and the measured particle size distributions. The solid circles correspond to samples with K/BC < 0.78, which are suspected to underestimate the BC concentration. For the data points for which the symbol size is equal to or greater than the error bar, the error bar has been omitted.

the optical depths of the smoke layers were computed and compared with those measured directly by the Sun photometers. Seven such data sets were obtained [*Hobbs*, 1996]. Optical depths derived from these two independent methods agreed to within 30% (J. L. Ross et al., unpublished data, 1998, (hereinafter referred to as R98)).

R98 also describe internal closure calculations using SCAR-B data. Particle size distributions measured from the C-131A aircraft were used as inputs to theoretical calculations of particle scattering, absorption, and mass concentrations. The calculated scattering and absorption were compared to direct measurements of these quantities at several discrete wavelengths. The calculated values were generally within ~25% of the measurements, with the former generally being slightly lower. The computations were then applied over the complete wavelength range of the solar spectrum. Parameterizations of the total scattering, scattering asymmetry, and absorption were derived. These are appropriate for use in radiative forcing calculations of regional smoke in Brazil as well as for remote sensing applications.

Using the parameterizations of the optical properties, radiative transfer theory was used to estimate the instantaneous and daily average direct radiative forcing of the regional hazes dominated by smoke in Brazil and their sensitivities to solar zenith angle, aerosol optical thickness, and surface type [*Ross and Hobbs*, this issue]. At point locations the daily average direct radiative forcing per unit optical depth (at $\lambda = 550$ nm) varied from -26 ± 6 W m^{-2} (cooling) over a dark surface to $+25 \pm 12$ W m^{-2} (warming) over a reflective surface.

Using SCAR-B data, *Ross and Hobbs* [this issue] have studied the effects of solar zenith angle, smoke optical thickness, and cloud properties on atmospheric heating rates. Daily heating rates of 3.5 K per day were calculated for a haze layer 3000 m thick with an optical thickness of 1 at a wavelength of 600 nm. Reductions due to regional hazes in Brazil of 30, 43, and 58% per day per unit optical depth were calculated for the total shortwave flux, photosynthetically active radiation, and total UV radiation, respectively. Similar reductions of irradiance were measured by *Eck et al.* [this issue].

7.5. Aerosol Radiative Model for Direct Radiative Forcing and Remote Sensing

7.5.1. Radiative model. The AERONET Sun photometer measurements from 1993 to 1995 were used to derive a self-consistent aerosol model that can be used as a basis for remote sensing of aerosol [*Kaufman et al.*, 1990, 1997] and for estimating the aerosol radiative forcing of climate [*Hobbs et al.*, 1997]. Remote sensing is limited in its capability to retrieve aerosol information. For example, inversion of spectral radiances from MODIS, to be launched on the NASA Earth Observing System in 1999, will include the aerosol optical thickness or mass concentration derived from radiances over dark land [*Kaufman et al.*, 1997]. Over the oceans, a two-parameter aerosol size distribution will also be retrieved [*Tanré et al.*, 1996, 1997]. Other aerosol optical and physical parameters have to be assumed, based on dynamic aerosol models [*Remer and Kaufman*, 1998] which describe the variability of the aerosol size distribution with aerosol loading. To be used for remote sensing, these models have to describe the whole vertical column and the properties of the ambient aerosol particles, which are derived from climatology of the AERONET sky data and compared with in situ properties [*Remer et al.*, 1997; *Ross et al.*, this issue]. Aerosol models have been developed for urban/industrial aerosol and, in this issue, for smoke aerosol [*Remer et al.*, this issue]. Table 3 summarizes the results and compares them with in situ measurements. While there is good agreement between the model based on the AERONET data and the in situ measurements of the particle size distribution, the single-scattering albedo (ω_0) of 0.9 at 660 nm used in the model is larger than the values measured in situ. Analysis of the variation of sky data with aerosol optical thickness at a scattering angle of 120° shows that a lower value of ω_0 (e.g., $\omega_0 = 0.85$) does not make a good fit [*Remer et al.*, this issue].

Two new techniques were applied to AERONET sky data to derive the aerosol real refractive index from the diffuse sky data at large scattering angles (80°–120°) [*Yamasoe et al.*, this issue] and to derive the aerosol single-scattering albedo by comparison of the sky-scattered solar radiation with the extinction of solar radiation from the direct solar beam [*Dubovik et al.*, this issue]. The results of these studies are also included in Table 3.

7.5.2. Optical properties and direct radiative forcing. To calculate direct aerosol radiative forcing, values of the following optical parameters are needed: mass light-scattering efficiency, the fraction of incident solar radiation backscattered by the aerosols, the single-scattering albedo, and the humidification factor. The University of Washington team used its C-131A aircraft to obtain extensive measurements of all four of these parameters for smoke in SCAR-B [*Hobbs et al.*, 1997; *Reid et al.*, this issue]. *Hobbs et al.* [1997] showed that if these measurements are applied to the simple model used by *Penner et al.* [1992], the derived magnitude of the globally averaged direct radiative forcing due to smoke from biomass burning worldwide is only -0.1 to -0.3 W m^{-2}, compared to -0.8 W m^{-2} estimated by *Penner et al.* [1992].

7.5.3. Application to remote sensing. Aircraft in situ and remote sensing measurements are not sufficiently frequent to document the spatial and temporal variability of aerosol loading, properties, and interactions with water vapor, clouds, and

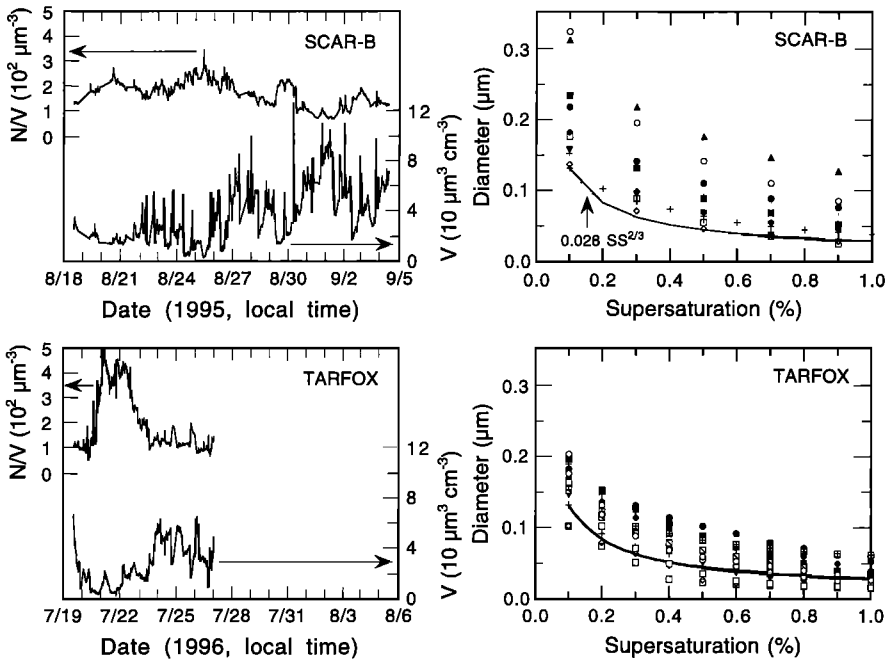

Figure 13. Results from ground-based measurements of the aerosol size distribution and CCN spectrum (after Ji et al., unpublished data, 1998). Time sequence of the ratio of the number of potential CCN (N) to the smoke aerosol volume (V) measured in (top left) Cuiabá, Brazil, and (bottom left) in Wallops, Virginia, during the TARFOX field experiment. N is defined as the number of particles with diameter $d \geq 0.1$ μm, V is the volume of part of the accumulation mode being measured (for $d \geq 0.6$ μm). The large change of the ratio N/V during TARFOX is due to a passage of a cold front that cleaned the air (low volumes) but generated a relatively high number of small particles. The critical diameter of particles activated in a given supersaturation (SS), d_c, is shown in (top right) for Brazil and (bottom right) for TARFOX. The Twomey expression ($d_c = 0.0028S^{-2/3}$) is shown for reference [*Twomey*, 1977].

radiation. Long-term monitoring of the variability of these quantities requires ground-based and spaceborne monitoring. However, because of the inherent complexity and assumptions involved in deriving aerosol properties from spaceborne measurements, precise evaluation of the techniques is required [e.g., *Vermote et al.*, 1997]. *Chu et al.* [this issue] applied the MODIS algorithm to derive the aerosol optical thickness from the MAS data recorded in SCAR-B over the AERONET Sun photometers and compared the results with the AERONET measurements. Using 17 such coincidental measurements, they concluded that the performance of the algorithm is better than anticipated, resulting in an error in the retrieved aerosol optical thickness ($\Delta\tau$) of $\pm 0.05 \pm 0.15\tau$. This result was obtained in spite of inherent errors in the ground-based measurements of aerosol optical thicknesses of ± 0.01 to $\pm$ 0.02 and an uncertainty in the MAS calibration that is larger than the anticipated uncertainty in the meticulously characterized and calibrated MODIS instrument [*Salomonson et al.*, 1989]. Application of a similar remote sensing technique to AVHRR data over Brazil in 1993 resulted in a similarly good agreement [*Vermote et al.*, 1997].

7.6. Aerosol Size Distribution, CCN, and Indirect Forcing

The low variability in the size distribution of aged smoke (i.e., smoke more than about 3 days old) is of significant importance for the estimation of its effect on cloud microstructures, reflectance, and indirect radiative forcing, and for remote sensing of this forcing [*Kaufman and Fraser*, 1997]. Aerosol models used to estimate aerosol forcing are based on information on source loading, evolution, and sinks of the aerosol mass (e.g., for sulfates see *Kiehl and Briegleb* [1993]). To estimate aerosol indirect forcing, the relationship between the number of CCN and their volume needs to be established. For sulfates, very nonlinear relationships have been used [*Boucher and Lohmann*, 1995; *Jones et al.*, 1994] due to the complex competition between gas phase and cloud phase oxidation of SO_2 into sulfate particles [*Langner et al.*, 1992; *Kaufman and Tanré*, 1994]. For smoke we anticipate the relationship between aerosol volume and CCN concentration to be more linear. In Cuiabá, Q. Ji et al. (unpublished data, 1998) measured the aerosol size distribution for $D < 0.6$ μm and the corresponding CCN spectrum. Similar instrumentation was used in the Tropospheric Aerosol Radiative Forcing Observational (TARFOX) experiment in Wallops, Virginia, in 1996 for urban/industrial aerosol. In Figures 13a and 13b the ratio of the number of potential CCN, N (particles with diameter >0.1 μm) to aerosol volume V (for diameter <0.6 μm) is plotted as a function of time for Cuiabá and Wallops, respectively. The variability of N/V is negatively correlated with V. The variability of N/V for the smoke aerosol is much smaller than that of urban/industrial aerosol. The main variation in N/V for the urban/industrial aerosol is between the aerosol properties before and after a passage of a front. The front cleans the atmosphere reducing the aerosol volume while generating the conditions for the formation of new aerosol particles. In Figures 13c and 13d the critical activation diameter d_c (i.e., the diameter, in μm, of the particle activated by a given supersaturation) is compared for Cuiabá and Wallops. The activation

diameter is calculated as the threshold diameter above which the number of particles is equal to the CCN concentration for the given supersaturation. The spectrum is compared with the empirical formula given by *Twomey* [1977]:

$$d_c = 0.028\ S^{-2/3} \quad (2)$$

where S is the supersaturation given in percent. While for smoke in Cuiabá the measured values of d_c are above the "Twomey" line, the results for TARFOX are mixed. This is in agreement with the lower hygroscopicity of smoke compared to that of urban/industrial aerosol.

The effects of smoke on cloud microphysics and reflectance have not been studied extensively yet using the SCAR-B data, but a previous study using AVHRR images over the same region in 1987 [*Kaufman and Nakajima*, 1993; *Kaufman and Fraser*, 1997] showed that aerosol effects on the cloud microphysics and reflectance is, on average, similar to the predictions of the Twomey model. This is in agreement with the small variability of the N/V ratio for smoke.

7.7. Surface Albedo and Surface Cover

Surface albedo is an important parameter in studying the interaction of solar radiation with the Earth. Anthropogenic changes in surface cover and its albedo affect the fraction of solar radiation reflected back to space and therefore constitute a radiative forcing of climate. The aerosol direct effect depends on the spectral relationship between surface bidirectional reflectance and the aerosol optical properties. The spectral bidirectional reflectance measurements by the CAR radiometer on the University of Washington C-131A aircraft contain very fine angular resolution (1° in zenith and <2° in azimuthal angles), and it is straightforward to compute the integrated hemispherical albedo for various types of surfaces (e.g., cerrado, dense forest, etc.). Comparing the computed albedo to the measured nadir reflectance (often used as a surrogate to the albedo in climate models), the nadir reflectance values underestimate the albedo generally by about 20%, with few extremes of up to 60%. Thus the analysis of CAR measurements during SCAR-B show that the estimation of spectral albedo from nadir reflectance produces large errors [*Tsay et al.*, this issue]. Remote sensing of the surface cover is affected by the presence of smoke. Several methods were suggested to overcome this problem. *Miura et al.* [this issue] uses AVIRIS data collected simultaneously with aerosol optical thickness measured from the ground during SCAR-B to compare several methods for remote sensing of the surface cover through the smoke.

8. Conclusions

The detailed measurements of smoke aerosol composition, size, and optical properties, reported in this issue, and summarized in Tables 2 and 3, have been used for preliminary estimates of direct and indirect radiative forcing by smoke [*Hobbs et al.*, 1997; *Kaufman and Fraser*, 1997]. The same parameters were measured or derived using several independent techniques. For example, several techniques were used to derive the aerosol absorption and black carbon concentration from laboratory analysis of filters, aircraft continuous in situ monitoring, and remote sensing from ground-based radiometers. More rigorous estimates of these forcings require documentation of the high spatial and temporal variability of smoke and its transport and dispersion over the globe. Such documentation is one of the objectives of the new satellite systems (e.g., POLDER on ADEOS, and MODIS and MISR on the NASA Earth Observing System to be launched in 1999). More detailed studies are needed of the effects of smoke on the properties of clouds.

Results from SCAR-B, and previous measurements, have been used to develop the capability of remote sensing of aerosol properties from the ground using Sun photometers. Detailed closure studies in SCAR-B have demonstrated general agreement between in situ and remote sensing measurements of smoke. The SCAR-B data have also been used to check the remote sensing of aerosol properties from satellites. Some understanding of the use of satellites to derive not only aerosol optical thickness but also aerosol mass loading and CCN concentrations has been initiated. New techniques for the use of satellites to expand remote sensing of fires to include measurements of the fire radiative energy for better quantifications of emissions were developed.

SCAR-B has continued previous efforts to estimate the emissions of trace gases and aerosol from fires, to understand the role of black carbon, and the effects of biomass burning on tropospheric ozone production.

Acknowledgments. Special thanks are due to the Brazilian government and Air Force, who went out of their way to make SCAR-B both successful and a pleasant experience. Special recognition goes to J. T. Suttles, previously at NASA Headquarters, for making SCAR-B happen. We thank L. G. M. Filho, head of Agencia Espacial Brasileira (Brazilian Space Agency), G. Shelton (NASA Ames Research Center), D. S. McDougal (NASA Langley Research Center), and A. Motta (INPE/Natal) for organizing the infrastructure of the experiment. The Brazilian Air Force observers: Capt. D. P. Damiao and Capt. N. S. de O. Andrade were superb guides through Brazil. We would like to thank J. Raposo from IBAMA for the logistical support for the meteorological center at IBAMA. The research reported in this paper was supported by the MODIS Science Team, the EOS Project Science Office, NASA's Radiation Science Program, the National Science Foundation, Environmental Protection Agency, the National Oceanic and Atmospheric Administration, and INPE.

References

Alvalá, P. C., and V. W. J. H. Kirchhoff, Observations of atmospheric methane and carbon monoxide in Brazil: SCAR-B mission, *J. Geophys. Res.*, this issue.

Alvalá, R. C. S., E. J. P. da Rocha, R. Gielow, J. R. Feitosa, J. B. M. Riberio, and G. Fisch, The atmospheric boundary layer experiment in Alta Floresta during the dry season 1995, in *SCAR-B Proceedings*, edited by V. W. J. H. Kirchhoff, pp. 5–8, Transtec, São Paulo, Brazil, 1996.

Anderson, B. E., W. B. Grant, G. L. Gregory, E. V. Browell, J. E. Collins Jr., G. W. Sachse, D. R. Bagwell, C. H. Hudgins, D. R. Blake, and N. J. Blake, Aerosol from biomass burning over the tropical South Atlantic region: Distribution and impacts, *J. Geophys. Res.*, *101*, 24,117–24,137, 1996.

Andreae, M. O., et al., Biomass burning emissions and associated haze layers over Amazonia, *J. Geophys. Res.*, *93*, 1509–1527, 1988.

Andreae, M. O., B. E. Anderson, D. R. Blake, J. D. Bradshaw, J. E. Collis, G. L. Gregory, G. W. Sachse, and M. C. Shipham, Influence of plumes from biomass burning on atmospheric chemistry over the equatorial and tropical South Atlantic during CITE 3, *J. Geophys. Res.*, *99*, 12,793–12,808, 1994.

Artaxo, P., H. Storms, F. Bruynseels, R. Van Grieken, and W. Maenhaut, Composition and sources of aerosols from the Amazon Basin, *J. Geophys. Res.*, *93*, 1605–1615, 1988.

Artaxo, P., W. Maenhaut, H. Storms, and R. Van Grieken, Aerosol characteristics and sources for the Amazon basin during the wet season, *J. Geophys. Res.*, *95*, 16,971–16,985, 1990.

Artaxo, P., F. Gerab, M. A. Yamasoe, and J. V. Martins, Fine mode aerosol composition in three long-term atmospheric monitoring

sampling stations in the Amazon Basin, *J. Geophys. Res.*, *99*, 22,857–22,868, 1994.

Artaxo, P., F. Gerab, M. A. Yamasoe, and J. V. Martins, *Global Biomass Burning*, edited by J. Levin, 519 pp., MIT Press, Cambridge, Mass., 1996.

Artaxo, P., F. Gerab, and M. A. Yamasoe, Long term atmospheric aerosol characterization in the Amazon Basin, in *Environmental Geochemistry in the Tropics*, edited by J. Wasserman, E. V. Silva Filho, and R. Villas Boas, pp. 227–250, Springer-Verlag, New York, 1997.

Artaxo, P., E. T. Fernandes, J. V. Martins, M. A. Yamasoe, P. V. Hobbs, W. Maenhaut, K. M. Longo, and A. Castanho, Large-scale aerosol source apportionment in Amazonia, *J. Geophys. Res.*, this issue.

Babbitt, R. E., D. E. Ward, R. A. Susott, P. Artaxo, and J. B. Kauffman, A comparison of concurrent airborne and ground based emissions generated from biomass burning in the Amazon Basin, in *SCAR-B Proceedings*, edited by V. W. J. H. Kirchhoff, pp. 23–27, Transtec, São Paulo, Brazil, 1996.

Browell, E. V., et al., Ozone and aerosol distributions and air mass characteristics over the South Atlantic basin during the burning season, *J. Geophys. Res.*, *101*, 24,043–24,068, 1996.

Boucher, O., and U. Lohmann, The sulfate-CCN-cloud albedo effect, a sensitivity study with two general circulation models, *Tellus*, *Ser-B*, *47*, 281–300, 1995.

Cachier, H., M. P. Brémond, and P. Baut-Ménard, Determination of atmospheric soot carbon with a simple thermal method, *Tellus*, *Ser B*, *41*, 379–390, 1989.

Castro, E. A., et al., Nutrient losses during biomass burning in Brazil, *J. Geophys. Res.*, in press, 1998.

Chu, D. A., Y. J. Kaufman, L. A. Remer, and B. N. Holben, Remote sensing of smoke from MODIS airborne simulator during SCAR-B experiment, *J. Geophys. Res.*, this issue.

Crutzen, P. J., and M. O. Andreae, Biomass burning in the tropics: Impact on atmospheric chemistry and biogeochemical cycles, *Science*, *250*, 1669–1678, 1990.

Crutzen, P. J., and J. W. Birks, The atmosphere after a nuclear war: Twilight at noon, *Ambio*, *11*, 114–125, 1982.

Crutzen, P. J., L. E. Heidt, J. P. Krasnec, W. H. Pollock, and W. Seiler, Biomass burning as a source of atmospheric gases: CO, H_2, N_2O, NO, CH_3Cl, and COS, *Nature*, *282*, 253–256, 1979.

Crutzen, P. J., A. C. Delany, J. Greenberg, P. Haagenson, L. Heidt, R. Lueb, W. Pollock, W. Seiler, A. Warburg, and P. Zimmerman, Tropospheric chemical composition measurements in Brazil during the dry season, *J. Atmos. Chem.*, *2*, 233–256, 1985.

Dubovik, O., B. N. Holben, Y. J. Kaufman, M. Yamasoe, A. Smirnov, D. Tanré, and I. Slutsker, Single-scattering albedo of smoke retrieved from sky radiance and solar transmittance from ground, *J. Geophys. Res.*, this issue.

Eck, T. F., B. N. Holben, I. Slutsker, and A. Setzer, Measurements of irradiance attenuation and estimation of aerosol single-scattering albedo for biomass burning aerosols in Amazonia, *J. Geophys. Res.*, this issue.

Ferek, R. J., J. S. Reid, P. V. Hobbs, D. R. Blake, and C. Liousse, Emission factors of hydrocarbons, halocarbons, trace gases, and particles from biomass burning in Brazil, *J. Geophys. Res.*, this issue.

Fishman, J., J. M. Hoell Jr., R. D. Bendura, R. J. McNeal, and V. W. J. H. Kirchhoff, NASA GTE TRACE A experiment (September–October 1992): Overview, *J. Geophys. Res.*, *101*, 23,865–23,880, 1996.

Freitas, S. R., K. M. Longo, M. A. F. Dias, and P. Artaxo, Numerical modeling of air mass trajectories from the biomass burning areas of the Amazon Basin, *Ann. Acad. Bras. Cienc.*, *68*, 193–206, 1996.

Gash, J. H. C., C. A. Nobre, J. M. Roberts, and R. L. Victoria (Eds.), *Amazon Deforestation and Climate*, John Wiley, New York, 1996.

Gleason, J. F., N. C. Hsu, and O. Torres, Biomass burning smoke measured using backscattered ultraviolet radiation: SCAR-B and Brazilian smoke interannual variability, *J. Geophys. Res.*, this issue.

Grace, J., J. Lloyd, J. McIntyre, A. C. Miranda, P. Meir, H. Miranda, C. Nobre, J. Moncrieff, J. Massheder, and Y. Malhi, Carbon dioxide uptake by an undisturbed tropical rain forest in SW Amazonia, 1992 to 1993, *Science*, *270*, 778–780, 1995.

Gregory, G. L., H. E. Fuelberg, S. P. Longmore, B. E. Anderson, J. E. Collins, and D. R. Blake, Chemical characteristics of tropospheric air over the tropical South Atlantic Ocean: Relationship to trajectory history, *J. Geophys. Res.*, *101*, 23,957–23,972, 1996.

Guild, L. S., J. B. Kauffman, L. J. Boeder, D. L. Cummings, E. A. Castro, R. E. Babbitt, and D. E. Ward, Dynamics associated with total aboveground biomass, carbon, nutrient pools, and biomass burning of primary forest and pastures in Rondônia, Brazil, *J. Geophys. Res.*, this issue.

Hao, W. M., and M.-H. Liu, Spatial and temporal distribution of tropical biomass burning, *Global Biol. Cycles*, *8*, 495–503, 1994.

Harriss, R. C., et al., The Amazon Boundary Layer Experiment (ABLE-2A): Dry season 1985, *J. Geophys. Res.*, *93*, 1351–1360, 1988.

Harriss, R. C., et al., The Amazon boundary layer experiment: Wet season 1987, *J. Geophys. Res.*, *95*, 16,721–16,736, 1990.

Herman, M., J. L. Deuzé, C. Devaux, P. Goloub, F. M. Bréon, and D. Tanré, Remote sensing of aerosol over land surfaces including polarization measurements and application to POLDER measurements, *J. Geophys. Res.*, *102*, 17,039–17,050, 1997a.

Herman, J. R., P. K. Bhartia, O. Torres, C. Hsu, C. Seftor, and E. Celarier, Global distribution of UV absorbing aerosol from Nimbus 7 TOMS data, *J. Geophys. Res.*, *102*, 16,911–16,922, 1987b.

Hobbs, P. V., Summary of types of data collected on the University of Washington's Convair C131-A aircraft in the Smoke, Clouds, and Radiation-Brazil (SCAR-B) field study from 17 August–20 September 1995, in *Report from the Cloud and Aerosol Research Group*, Dep. of Atmos. Sci., Univ. of Wash., Seattle, 1996. (Available on the web at http://cargsun2.atmos.washington.edu.)

Hobbs, P. V., and L. F. Radke, Cloud condensation nuclei from a simulated forest fire, *Science*, *163*, 279–280, 1969.

Hobbs, P. V,. J. S. Reid, J. A. Herring, J. D. Nance, R. E. Weiss, J. L. Ross, D. A. Hegg, R. D. Ottmar, and C. Liousse, Particle and trace gas measurements in the smoke from prescribed burns of forest products in the Pacific Northwest, in *Biomass Burning and Global Change*, edited by J. S. Levine, pp. 697–715, MIT Press, Cambridge, Mass., 1996.

Hobbs, P. V., J. S. Reid, R. A. Kotchenruther, R. J. Ferek, and R. Weiss, Direct radiative forcing by smoke from biomass burning, *Science*, *275*, 1776–1778, 1997.

Holben, B. N., Y. J. Kaufman, D. Tanré, and D. E. Ward, Optical properties of aerosol from biomass burning in the tropics: BASE-A, in *Global Biomass Burning*, pp. 403–411, MIT Press, Cambridge, Mass., 1991.

Holben, B. N., A. Setzer, T. F. Eck, A. Pereira, and I. Slutsker, Effect of dry season biomass burning on Amazon Basin aerosol concentrations and optical properties, 1992–1994, *J. Geophys. Res.*, *101*, 19,455–19,464, 1996.

Holben, B. N., et al., Automatic sun and sky scanning radiometer systems for network and aerosol monitoring, *Remote Sens. Environ.*, in press, 1998.

Hsu, N. C., J. R. Herman, P. K. Bhartia, C. J. Seftor, O. Torres, A. M. Thompson, J. F. Gleason, T. F. Eck, and B. N. Holben, Detection of biomass burning smoke from TOMS measurements, *Geophys. Res. Lett.*, *23*, 745–748, 1996.

Husar, R. B., J. Prospero, and L. L. Stowe, and L. L. Stowe, Characterization of tropospheric aerosols over the oceans with the NOAA-AVHRR aerosol optical thickness operational product, *J. Geophys. Res.*, *102*, 16,889–16,909, 1997.

Intergovernmental Panel on Climate Change (IPCC), *Radiative Forcing of Climate Change*, Cambridge Univ. Press, New York, 1995.

Jones, A., D. L. Roberts, and A. Slingo, A climate model study of indirect radiative forcing by anthropogenic sulphate aerosols, *Nature*, *370*, 450–453, 1994.

Kahn, R., R. West, D. McDonald, B. Rheingans, and M. I. Mishchenko, Sensitivity of multiangle remote sensing observations to aerosol sphericity, *J. Geophys. Res.*, *102*, 16,861–16,870, 1997.

Kaufman, Y. J., and R. S. Fraser, Confirmation of the smoke particles effect on clouds and climate, *Science*, *277*, 1636–1639, 1997.

Kaufman, Y. J., and B. N. Holben, Hemispheric backscattering by biomass burning and sulfate particles derived from sky measurements, *J. Geophys. Res.*, *101*, 19,433–19,445, 1996.

Kaufman, Y. J., and T. Nakajima, Effect of Amazon smoke on cloud microphysics and albedo, *J. Appl. Meteorol.*, *32*, 729–744, 1993.

Kaufman, Y. J., and D. Tanré, Variations in cloud supersaturation and the aerosol indirect effect on climate, *Nature*, *369*, 45–48, 1994.

Kaufman, Y. J., C. J. Tucker, and I. Fung, Remote sensing of biomass burning in the tropics, *J. Geophys. Res.*, *95*, 9927–9939, 1990.

Kaufman, Y. J., A. Setzer, D. Ward, D. Tanre, B. N. Holben, P. Menzel, M. C. Pereira, and R. Rasmussen, Biomass burning air-

borne and spaceborne experiment in the Amazonas (BASE-A), *J. Geophys. Res.*, *97*, 14,581–14,599, 1992.

Kaufman, Y. J., B. N. Holben, D. Tanré, and D. Ward, Remote sensing of biomass burning in the Amazon, *Rem. Sens. Rev.*, *10*, 51–90, 1994.

Kaufman, Y. J., D. Tanré, L. Remer, E. Vermote, A. Chu, and B. N. Holben, Remote sensing of tropospheric aerosol from EOS-MODIS over the land using dark targets and dynamic aerosol models, *J. Geophys. Res.*, *102*, 17,051–17,067, 1997.

Kaufman, Y. J., C. Justice, L. Flynn, J. D. Kendall, E. M. Prins, L. Giglio, D. E. Ward, W. P. Menzel, and A. W. Setzer, Potential global fires monitoring from EOS-MODIS, *J. Geophys. Res.*, in press, 1998.

Kaufman, Y. J., R. Kleidman, M. D. King, and D. E. Ward, SCAR-B fires in the tropics: Properties and remote sensing from EOS-MODIS, *J. Geophys. Res.*, this issue.

Kiehl, J. T., and B. P. Briegleb, The relative roles of sulfate aerosols and greenhouse gases in climate forcing, *Science*, *260*, 311–314, 1993.

King, M. D., M. G. Strange, P. Leone, and L. R. Blaine, Multiwavelength scanning radiometer for airborne measurements of scattered radiation within clouds, *J Atmos. Oceanic Technol.*, *3*, 513–522, 1986.

King, M. D., et al., Airborne scanning spectrometer for remote sensing of cloud, aerosol, water vapor and surface properties, *J. Atmos. Oceanic Technol.*, *13*, 777–794, 1996.

King, M. D., S. C. Tsay, S. A. Ackerman, and N. F. Larsen, Discriminating heavy aerosol, clouds, and fires during SCAR-B: Application of airborne multispectral MAS data, *J. Geophys Res.*, this issue.

Kirchhoff, V. W. L. H., Are the northern hemispheric ozone densities larger?, *Eos Trans. AGU*, *65*, 440, 1984.

Kirchhoff, V. W. J. H., Surface ozone measurements in Amazonia, *J. Geophys. Res.*, *93*, 1469–1476, 1988.

Kirchhoff, V. W. J. H., Increasing concentrations of CO and O_3-rising deforestation rates and increasing tropospheric carbon monoxide and ozone in Amazonia, *Environ. Sci. Pollut. Res.*, *3*, 210–212, 1996.

Kirchhoff, V. W. J. H., and P. C. Alvalá, Overview of an aircraft expedition into the Brazilian cerrado for the observation of atmospheric trace gases, *J Geophys Res*, *101*, 23,973–23,981, 1996.

Kotchenruther, R A. and P. V. Hobbs, Humidification factors of aerosols from biomass burning in Brazil, *J. Geophys. Res.*, this issue.

Kotchenruther, R. A., P. V. Hobbs, and D. A. Hegg, Humidification factors for atmospheric aerosols off the mid-Atlantic coast of the United States, *J Geophys. Res.*, in press, 1998.

Kuhlbusch, T. A. J., M. O. Andreae, H. Cachier, J. G. Goldammer, J. P. Lacaux, R. Shea, and P. J. Crutzen, Black carbon formation by savanna fires: Measurements and implications for the global carbon cycle, *J. Geophys Res.*, *101*, 23,651–23,666, 1996.

Lacaux, J. P., J. M. Brustet, R. Delmas, J. C. Menaut, L. Abbadie, B. Bonsang, H. Cachier, J. Baudet, M. O. Andreae, and G. Helas, Biomass burning in the tropical savannas of Ivory Coast: An overview of the field experiment Fire of Savannas (FOS/DECAFE 91), *J. Atmos. Chem.*, *22*, 195–216, 1995.

Lacaux, J. P., R. Delmas, and C. Jambert, NO_x emissions from African savanna fires, *J. Geophys. Res.*, *101*, 23,585–23,595, 1996.

Langner, J., H. Rodhe, P. J. Crutzen, and P. Zimmermann, Anthropogenic influence on the distribution of tropospheric sulphate aerosol, *Nature*, *359*, 712–715, 1992.

Le Canut, P. M., M. O. Andreae, G. W. Harris, F. G. Wienhold, and T. Zeker, Aerosol optical properties over Southern Africa during SAFARI-92, in *Biomass Burning and Global Change*, edited by J. S. Levine, MIT Press, Cambridge, Mass., 1996.

Liousse, C., J. E. Penner, C. Chuang, J. J. Walton, H. Eddleman, and H. Cachier, A global 3-D model of carbonaceous aerosol, *J. Geophys. Res.*, *101*, 19,411–19,432, 1996.

Lindesay, J. A., M. O. Andreae, J. G. Goldammer, G. Hariss, H. J. Annegarn, M. Garstang, R. J. Scholes, and B. W. van Wilgen, IGBP global atmospheric chemistry SAFARI-92 field experiment: Background and overview, *J. Geophys. Res.*, *101*, 23,521–23,530, 1996.

Lobart, J. M., M. Scharffe, W. M. Hao, T. A. Kuhlbusch, R. Seuwen, P. Warneck, and P. J. Crutzen, Experimental evaluation of biomass burning emissions: Nitrogen and carbon containing compounds, in *Biomass Burning and Global Change*, edited by J. S. Levine, pp. 289–304, MIT Press, Cambridge, Mass., 1991.

Logan, J. A., and V. W. J. H. Kirchhoff, Seasonal variation in tropospheric ozone at Natal Brazil, *J. Geophys. Res.*, *91*, 7875–7882, 1986.

Longo, K. M., A. M. Thompson, V. Kirchhoff, and P. Artaxo, Correlation between smoke and tropospheric ozone concentrations in Cuiabá during SCAR-B, *J. Geophys. Res.*, in press, 1998.

Maenhaut, W., I. Salam, J. Cafmeyer, H. J. Annegarn, and M. O. Andreae, Regional atmospheric aerosol composition and sources in the eastern Transvaal, South Africa, and the impact of biomass burning, *J. Geophys. Res.*, *101*, 23,651–23,666, 1996.

Martins, J. V., P. Artaxo, C. Liousse, J. S. Reid, P. V. Hobbs, and Y. J. Kaufman, Effects of black carbon content, particle size, and mixing on light absorption by aerosol particles from biomass buring in Brazil, *J. Geophys. Res.*, this issue (a).

Martins, J. V., P. V. Hobbs, R. E. Weiss, and P. Artaxo, Shapes of smoke particles from biomass burning in Brazil, *J. Geophys. Res.*, this issue (b).

Martonchik, J. V.l, and D. J. Diner, Retreival of aerosol and land surface optical properties from multi-angle satellite imagery, *IEEE Trans. Geosci. Remote Sens.*, *30*, 223–230, 1992.

Mello-Ivo, W., S. Ferreira, Y. Biot, and S. Ross, Nutrients in soil solution following selective logging of a humid tropical 'terra firme' forest north of Manaus, Brazil, *Environ. Geochem. Health*, *18*, 69–75, 1996.

Miura, T., A. R. Huete, W. J. D. van Leeuwen, and K. Didan, Vegetation detection through smoke-filled AVIRIS images: An assessment using MODIS band passes, *J. Geophys. Res.*, this issue.

Nakajima, T., G. Tonna, R. Rao, P. Boi, Y. Kaufman, and B. Holben, Use of sky brightness measurements from ground for remote sensing of particulate polydispersions, *Appl. Opt.*, *35*, 2672–2686, 1996.

Nobre, C. A., L. F. Mattos, C. P. Dereczynski, T. A. Tarasova, and I. V. Trosnikov, Overview of atmospheric conditions during the Smoke, Clouds, and Radiation-Brazil (SCAR-B) field experiment, *J. Geophys. Res.*, this issue.

Novakov, T., and C. E. Corrigan, Thermal characterization of biomass smoke particles, *Mikrochim. Acta*, *119*, 157–166, 1995.

Novakov, T., D. A. Hegg, and P. V. Hobbs, Airborne measurements of carbonaceous aerosols off the East Coast of the United States, *J. Geophys. Res.*, *102*, 30,023–30,030, 1997.

Penner, J. E., R. E. Dickinson, and C. A. O'Neill, Effects of aerosol from biomass burning on the global radiation budget, *Science*, *256*, 1432–1433, 1992.

Pereira, E. B., A. W. Setzer, F. Gerab, P. E. Artaxo, M. C. Pereira, and G. Monroe, Airborne measurements of aerosol from biomass burning in Brazil related to the TRACE-A experiment, *J. Geophys. Res.*, *101*, 23,983–23,992, 1996.

Pickering, K. E., et al., Convective transport of biomass burning emissions over Brazil during TRACE A, *J. Geophys. Res.*, *101*, 23,993–24,012, 1996.

Prins, E. M., and W. P. Menzel, Investigation of biomass burning and aerosol loading and transport utilizing geostationary satellite data, in *Biomass Burning and Global Change*, edited by J. S. Levine, pp. 65–72, MIT Press, Cambridge, Mass., 1996.

Prins, E. M., J. M. Feltz, W. P. Menzel, and D. E. Ward, An overview of GOES 8 diurnal fire and smoke results for SCAR-B and the 1995 fire season in South America, *J. Geophys. Res.*, this issue.

Radke, L. F., Airborne observations of cloud microphysics modified by anthropogenic forcing, in *Symposium on Atmospheric Chemistry and Global Climate*, Am. Meteorol. Soc., Boston, Mass., 1989.

Radke, L. F., D. A. Hegg, P. V. Hobbs, J. D. Nance, J. H. Lyons, K. K. Laursen, R. E. Weiss, P. J. Riggan, and D. W. Ward, Particulate and trace gas emissions from large biomass fires in North America, in *Global Biomass Burning*, pp. 209, MIT Press, Cambridge, Mass., 1991.

Reid, J. S., and P. V. Hobbs, Physical and optical properties of young smoke from individual biomass fires in Brazil, *J. Geophys. Res.*, this issue.

Reid, J. S., P. V. Hobbs, R. F. Ferek, D. Blake, J. V. Martins, M. R. Dunlop, and C. Liousse, Physical, chemical, and optical properties of regional hazes dominated by smoke in Brazil, *J. Geophys. Res.*, this issue (a).

Reid, J. S., P. V. Hobbs, C. Liousse, J. V. Martins, R. E. Weiss, and T. F. Eck, Comparisons of techniques for measuring shortwave absorption and black carbon content of aerosol from biomass burning in Brazil, *J. Geophys. Res.*, this issue (b).

Remer, L. A., and Y. J. Kaufman, Dynamic aerosol model: Urban industrial aerosol, *J. Geophys. Res.*, *103*, 13,859–13,871, 1998.

Remer, L. A., Y. J. Kaufman, and B. N. Holben, The size distribution of ambient aerosol particles: Smoke vs. urban/industrial aerosol, in

Global Biomass Burning, edited by J. Levin, 519 pp., MIT Press, Cambridge, Mass., 1996.

Remer, L. A., S. Gassó, D. Hegg, Y. J. Kaufman, and B. N. Holben, Urban/industrial aerosol: Ground-based Sun/sky radiometer and airborne in situ measurements, *J. Geophys. Res.*, *102*, 16,849–16,859, 1997.

Remer, L. A., Y. J. Kaufman, B. N. Holben, A. M. Thompson, and D. McNamara, Biomass burning aerosol size distribution and modeled optical properties, *J. Geophys. Res.*, this issue.

Richey, J. E., J. I. Hedges, A. H. Devol, P. D. Quay, R. L. Victoria, L. A. Martinelli, and B. R. Forsberg, Biogeochemistry of carbon in the Amazon River, *Limnol. Oceanogr.*, *35*, 353–371, 1990.

Robock, A., Enhancement of surface cooling due to forest fire smoke, *Science*, *242*, 911–913, 1988.

Ross, J. L., and P. V. Hobbs, Radiative characteristics of regional hazes dominated by smoke from biomass burning in Brazil: Closure tests and direct radiative forcing, *J. Geophys. Res.*, this issue.

Salomonson, V. V., W. L. Barnes, P. W. Maymon, H. E. Montgomery, and H. Ostrow, MODIS: Advanced facility instrument for studies of the earth as a system, *IEEE Trans. Geos. Remote Sens.*, *27*, 145–153, 1989.

Seinfeld, J. H., et al., Aerosol radiative forcing and climate change, a plan for research, National Acad. Press, Washington, D. C., 1996.

Setzer, A. W., and M. C. Pereira, Amazonian biomass burning in 1987 and an estimate of their tropospheric emissions, *Ambio*, *20*, 19–22, 1991.

Skole, D., and C. J. Tucker, Tropical deforestation and habitat fragmentation in the Amazon: Satellite data from 1978 to 1988, *Science*, *260*, 1905–1910, 1993.

Spinhirne, J. D., M. Z. Hansen, and L. O. Caudill, Cloud top remote sensing by airborne lidar, *Appl. Opt.*, *22*, 1564–1571, 1982.

Swap, R., M. Garstang, S. A. Macko, P. D. Tyson, W. Maenhaut, P. Artaxo, P. Kållberg, and R. Talbot, The long-range transport of southern African aerosols to the tropical South Atlantic, *J. Geophys. Res.*, *101*, 23,777–23,792, 1996.

Tanré, D., M. Herman, and Y. J. Kaufman, Information on aerosol size distribution contained in solar reflected radiances, *J. Geophys. Res.*, *101*, 19,043–19,060, 1996.

Tanré, D., Y. J. Kaufman, M. Herman, and S. Mattoo, Remote sensing of aserosol properties over oceans MODIS/EOS spectral radiances, *J. Geophys. Res.*, *102*, 16,971–16,988, 1997.

Thompson, A. M., et al., Ozone over southern Africa during SAFARI-92/TRACE A, *J. Geophys. Res.*, *101*, 23,793–23,808, 1996.

Torres, O., P. K. Bhartia, J. R. Herman, Z. Ahmad, and J. F. Gleason, Derivation of aerosol properties from satellite measurements of backscattered ultraviolet radiation: Theoretical basis, *J. Geophys. Res.*, *103*, 17,099–17,110, 1998.

Tsay, S.-C., M. D. King, G. T. Arnold, and J. Y. Li, Airborne spectral measurements of surface anisotropy during SCAR-B, *J. Geophys. Res.*, this issue.

Twomey, S., The influence of pollution on the short wave albedo of clouds, *J. Atmos. Sci.*, *34*, 1149–1152, 1977.

Vane, G., R. O. Green, T. G. Chrien, H. T. Enmark, E. G. Hansen, and W. M. Porter, The airborne visible/infrared imaging spectrometer (AVIRIS), *Remote Sens. Environ.*, *44*, 127–143, 1993.

Vermote, E. F., N. El Saleous, C. O. Justice, Y. J. Kaufman, J. L. Privette, L. Remer, J. C. Roger, and D. Tanré, Atmospheric correction of visible to mid-IR EOS-MODIS data over land surface, background, operational algorithm, and validation, *J. Geophys. Res.*, *102*, 17,131–17,141, 1997.

von Hoyningen-Huene, W., T. Schmidt, and C. A. Kee, Climate relevant aerosol parameters of South East Asia forest fire haze, paper presented at the International Symposium on the Atmospheric Correction of Satellite Data and its Application to Global Environment, Chiba, Japan, 1998.

Ward, D. E., and C. C. Hardy, Smoke emissions from wild land fires, *Environ. Int.*, *17*, 117–134, 1991.

Ward, D. E., R. Susott, J. Kauffman, R. Babbitt, B. N. Holben, Y. J. Kaufman, A. Setzer, R. Rasmussen, D. Cumming, and B. Dias, Emissions and burning characteristics of biomass fires for cerrado and tropical forest regions of Brazil—BASE-B experiment, *J. Geophys. Res.*, *97*, 14,601–14,619, 1992.

Ward, D. E., W. M. Hao, R. A. Susott, R. E. Babitt, R. W. Shea, J. B. Kauffman, and C. O. Justice, Effects of fuel composition on combustion efficiency and emission factors for African savanna ecosystem, *J. Geophys. Res.*, *101*, 23,569–23,576, 1996.

Warner, J., and S. Twomey, The production of cloud nuclei by cane fires and the effect on cloud droplet concentration, *J. Atmos. Sci.*, *24*, 704–706, 1967.

Yamasoe, M. A., Y. J. Kaufman, O. Dubovik, L. A. Remer, B. Holben, and P. Artaxo, Retrieval of the real part of the refractive index of smoke particles from Sun/sky measurements during SCAR-B, *J. Geophys. Res.*, this issue.

P. Artaxo, and K. M. Longo, Instituto de Fisica, Universidade de São Paulo, Caixa Postal 66318, CEP 05389-970, São Paulo, SP, Brazil.

S. A. Christopher, Department of Atmospheric Sciences, University of Alabama in Huntsville, 977 Explorer Boulevard, Huntsville, AL 35899.

J. F. Gleason, Y. J. Kaufman, L. A. Remer, J. D. Spinhirne, A. M. Thompson, and S.-C. Tsay, Laboratory for Atmospheres, NASA Goddard Space Flight Center, Mail Code 913, Greenbelt, MD 20771. (e-mail: kaufman@climate.gsfc.nasa.gov).

P. V. Hobbs, Department of Atmospheric Sciences, University of Washington, Box 351640, Seattle, WA 98195-1640.

B. N. Holben, Laboratory for Terrestrial Physics, NASA Goddard Space Flight Center, Greenbelt, MD 20771.

Q. Ji, Science Systems and Applications Inc., 5900 Princess Garden Parkway, Lanham, MD 20706.

M. D. King, Earth Sciences Directorate, NASA Goddard Space Flight Center, Greenbelt, MD 20771.

V. W. J. H. Kirchhoff, L. F. Mattos, and C. A. Nobre, INPE, Caixa Postal 515, Ave. Dos Astronautas, 1758, São José dos Campos, SP 12201-970, Brazil.

E. M. Prins, NOAA/NESDIS/ORA, 1225 West Dayton St., Madison, WI 53706.

D. E. Ward, Intermountain Research Station, Forest Service, USDA, Missoula, MT 59807.

(Received September 11, 1997; revised April 16, 1998;
accepted June 22, 1998.)